**University of Alberta**

# Mathematical model of bursting electrical activity of pancreatic $\beta$-cells in response to glucose diffusion

by

Lisa Corscadden

A thesis submitted to the Faculty of Graduate Studies and Research in partial fulfillment of the requirements for the degree of Master of Science in Applied Mathematics

Department of Mathematical Sciences

Edmonton, Alberta

Fall 2000

National Library of Canada
Acquisitions and Bibliographic Services
395 Wellington Street
Ottawa ON K1A 0N4
Canada

Bibliothèque nationale du Canada
Acquisitions et services bibliographiques
395, rue Wellington
Ottawa ON K1A 0N4
Canada

*Your file Votre référence*

*Our file Notre référence*

The author has granted a non-exclusive licence allowing the National Library of Canada to reproduce, loan, distribute or sell copies of this thesis in microform, paper or electronic formats.

L'auteur a accordé une licence non exclusive permettant à la Bibliothèque nationale du Canada de reproduire, prêter, distribuer ou vendre des copies de cette thèse sous la forme de microfiche/film, de reproduction sur papier ou sur format électronique.

The author retains ownership of the copyright in this thesis. Neither the thesis nor substantial extracts from it may be printed or otherwise reproduced without the author's permission.

L'auteur conserve la propriété du droit d'auteur qui protège cette thèse. Ni la thèse ni des extraits substantiels de celle-ci ne doivent être imprimés ou autrement reproduits sans son autorisation.

0-612-59792-X

Canada

**University of Alberta**

**Library Release Form**

**Name of Author:** Lisa Corscadden

**Title of Thesis:** Mathematical model of bursting electrical activity of pancreatic $\beta$-cells in response to glucose diffusion

**Degree:** Master of Science

**Year this Degree Granted:** 2000

Permission is hereby granted to the University of Alberta to reproduce single copies of this thesis and to lend or sell such copies for private, scholarly or scientific research purposes only.

The author reserves all other publication and other rights in association with the copyright in the thesis, and except as herein before provided, neither the thesis nor any substantial portion thereof may be printed or otherwise reproduced in any material form whatever without the author's prior written permission.

Lisa Corscadden

BOX 280,
Windthorst, Saskatchewan, Canada
S0G 5G0

Date July 31, 2000

## Abstract

Pancreatic islets consist of hundreds of $\beta$-cells, coupled together electrically. In response to glucose, $\beta$-cells exhibit a pattern of electrical activity called bursting, correlated with insulin release. In experimental settings, glucose enters the islet through hindered diffusion. Therefore, $\beta$-cells within an islet are not always exposed to a uniform glucose distribution. However, their electrical activity appears to be synchronized.

The focus of this thesis is the development of a model describing the initiation of bursting electrical activity in an islet in response to diffusing glucose. We quantify the observed delay in the onset of bursting in terms of the glucose bath concentration the islet is exposed to, and coupling conductance between neighbouring cells. We find that the delay increases with coupling conductance and decreases with glucose bath concentration. We show that the average glucose concentration necessary to induce bursting is lower in an islet than in a single cell.

**University of Alberta**

**Faculty of Graduate Studies and Research**

The undersigned certify that they have read, and recommend to the Faculty of Graduate Studies and Research for acceptance, a thesis entitled **Mathematical model of bursting electrical activity of pancreatic $\beta$-cells in response to glucose diffusion** submitted by **Lisa Corscadden** in partial fulfillment of the requirements for the degree of Master of Science in Applied Mathematics.

Gerda de Vries

Prof. G. de Vries

M. Klobukowski

Prof. M. Klobukowski

P. Minev

Prof. P. Minev

Date: July 26, 2002

## Acknowledgement

Sincerest thanks to my supervisor, Gerda de Vries, for her patience, guidance, and for setting a wonderful example throughout the course of this research. You inspire me to dream bigger. Also :> to the members of the math biology group for helpful comments, attentive ears, and continued support. Finally, thanks to my family, immediate and extended, and close friends, for believing in me when I did not.

# Contents


**1 Introduction** **1**

1.1 Cell electrophysiology . . . . . 4

1.1.1 Mathematical modelling of electrophysiological phenomena 7

1.2 Electrophysiology of $\beta$-cells . . . . . 11

1.2.1 Single $\beta$-cell model . . . . . 13

1.2.2 Electrophysiological effects of glucose . . . . . 17

1.3 Glucose diffusion . . . . . 20

1.4 Thesis outline . . . . . 26

**2 Development of the Combined Model** **28**

2.1 Discrete gap junctional coupling . . . . . 29

2.2 Continuum model . . . . . 31

2.3 Development of the connection between the islet electrical activity model and the model of glucose diffusion . . . . . 32

2.4 Combined model . . . . . 34

2.5 Numerical methods . . . . . 35

**3 Results from the Combined Model** **39**

3.1 Delay in onset of electrical activity . . . . . 40

3.2 Effect of coupling strength on the delay . . . . . 43

3.3 Effect of glucose bath concentration on the delay . . . . . 46

3.4 Effect of the islet radius on the delay . . . . . 51
3.5 Average glucose concentration within the islet at the onset of bursting 55
3.6 Several step changes in the glucose bath concentration . . . . . 58

**4 Discussion and Conclusions** **61**

**Bibliography** **64**

# List of Tables

1.1 Parameter values for the single $\beta$-cell model . . . . . 16
1.2 Parameter values for the glucose diffusion model . . . . . 24

2.1 Parameter values for the combined model . . . . . 36

# List of Figures


1.1 Experimentally observed action potential . . . . . 6

1.2 Steady-state curves of the Hodgkin and Huxley gating variables . 11

1.3 Parts of a burst . . . . . 12

1.4 Typical burst and corresponding slow variable oscillation . . . . . 17

1.5 Effects of changing glucose on single $\beta$-cell electrical activity . . . 19

1.6 Intracellular and extracellular glucose throughout an islet at various times . . . . . 25

2.1 The relationship between glucose and the glucose sensing parameter $R$ . . . . . 33

3.1 Example of a delay in the onset of electrical activity after a stimulatory glucose bath is introduced . . . . . 41

3.2 Weighted-average glucose distribution throughout the islet at various times . . . . . 42

3.3 Examples in the delay in the onset of islet electrical activity for various values of $D$ . . . . . 44

3.4 Weighted-average glucose distribution at the onset of bursting for various values of the parameter $D$ . . . . . 45

3.5 Delay in the onset of islet electrical activity as a function of the parameter $D$ . . . . . 47

3.6 Examples of the delay in onset of islet electrical activity as the glucose bath concentration is varied . . . . . 48
3.7 Islet bursting electrical activity for a glucose bath concentration of 16.5 mM . . . . . 49
3.8 Weighted-average glucose distribution at the onset of bursting for a glucose bath concentration of 16.5 mM . . . . . 50
3.9 Delay in the onset of islet electrical activity as a function of the glucose bath concentration . . . . . 51
3.10 Delay in the onset of bursting and glucose distributions in the outer shells for an islet of radius 200 $\mu$m . . . . . 52
3.11 Delay in the onset of islet electrical activity as a function of the glucose bath concentration for different sized islets . . . . . 53
3.12 Weighted-average glucose distribution at the onset of bursting for islet of radius 200 $\mu$m . . . . . 54
3.13 Weighted-average glucose throughout the islet at the onset of bursting as coupling strength is varied . . . . . 56
3.14 Weighted-average glucose throughout the islet at the onset of bursting as a function of the glucose bath concentration . . . . . 57
3.15 Observed bursting behaviour for several step changes in the glucose bath concentration . . . . . 59

# Chapter 1

# Introduction

Blood glucose level is maintained by hormones secreted in the pancreas. Insulin, secreted by $\beta$-cells in the pancreas, is produced in response to a rise in glucose in the blood plasma occurring after a meal for example. Insulin then alerts target tissues, such as muscle and liver tissue, indicating that glucose is available to be stored or used as fuel. As glucose levels in the blood decline, insulin secretion decreases and cells return to using stored energy. Defects in the glucose-insulin feedback loop can cause serious complications, such as diabetes.

In Type 1 diabetes, also referred to as early-onset or juvenile diabetes, the immune system attacks and kills the pancreatic $\beta$-cells that produce insulin for the body. People with Type 1 diabetes do not produce any insulin and must carefully monitor their blood sugar levels, taking insulin to control them. There is no cure, and failure to control blood sugar levels can cause blindness, loss of limbs and early death.

Type 2, or late-onset diabetes, involves several components. Among the contributing factors is that the body does not properly respond to the insulin it produces. Decreased insulin levels, caused by a deficit in $\beta$-cell mass, or defects in $\beta$-cells themselves, are also associated with Type 2 diabetes. Late-onset di-

abetes represents the majority of the occurrences of the disease, and can often be controlled with a regulated diet and exercise program. If not, drugs that increase insulin secretion or insulin injections are used to treat the disease. Thus, the importance of $\beta$-cells in insulin secretion motivates further study of $\beta$-cells in particular. The events occurring in $\beta$-cells resulting in insulin secretion will be our focus here.

$\beta$-cells form clusters referred to as islets of Langerhans. The membrane potential of the electrically excitable $\beta$-cells exhibits a pattern of oscillatory behavior when exposed to a stimulatory glucose concentration. Electrical gap junctions connect most neighbouring $\beta$-cells in the islet, and act to synchronize the pattern of electrical activity. This pattern, known as bursting, is characterized by a silent phase, where the membrane potential changes only slowly, followed by an active phase, where the membrane potential oscillates rapidly. As glucose concentration increases, the active phase lengthens and the silent phase shortens. Insulin is secreted during the active phase. Thus, $\beta$-cell electrical activity is a critical component of the glucose-induced insulin secretion process. Therefore, the study of the electrical behaviour of $\beta$-cells is motivated by the prospect of gaining a better understanding of insulin release.

The first mathematical model of bursting in a single $\beta$-cell was developed by Chay and Keizer in 1983 [8]. Despite the unavailability of complete electrophysiological data, this preliminary model was successful at simulating the bursting phenomenon. As new information became available and biophysical theories were modified, several different models arose. Still, several questions remain, and there is no consensus on one correct model. Therefore, in this thesis we restrict our attention to a generic model that possesses the minimal characteristics for bursting and can be easily adapted as necessary.

It was originally assumed that the single-cell models were representative of

the behaviour of islet cells coupled tightly together. However, most experimental reports describe bursting only in large clusters of $\beta$-cells or islets [22], not in single cells. There is also experimental evidence that coupling enhances insulin secretion [11]. Therefore, we use the generic $\beta$-cell model to develop a three dimensional islet model, incorporating electrical gap junctions in order to reflect the significance of the organization of $\beta$-cells into an islet, as in [19].

The role of glucose diffusion in $\beta$-cell electrical activity within an islet was investigated extensively by Bertram and Pernarowski in 1998 [6]. A model of glucose diffusion through an islet was developed. They found that the time required for glucose to diffuse into an islet could be significant in accounting for the delay in electrical activity observed experimentally after an islet is exposed to a stimulatory glucose bath.

The goal in this thesis is to combine these two major pieces of the puzzle, namely the dynamics of islet electrical activity, and the process of glucose diffusion throughout the islet, in order to achieve an understanding of islet dynamics on a broader scale. To accomplish this goal, we must first understand both $\beta$-cell electrophysiology and glucose diffusion individually. The remainder of the introductory chapter is devoted to describing in detail the necessary background information.

In Section 1.1, general cell electrophysiology will be discussed. The electrophysiology of $\beta$-cells is considered in Section 1.2, where the generic single-cell model is explained. In Section 1.3, we turn our attention to the issue of glucose diffusion. This section includes a summary of the work done by Bertram and Pernarowski regarding glucose diffusion in an islet and the development of a glucose diffusion model. Finally, the questions addressed by this thesis and an outline of the major topics to be discussed in the remainder of the thesis are expressed in Section 1.4.

## 1.1 Cell electrophysiology

All cells are enclosed by a thin membrane made up of phospholipid molecules. The membrane structure is formed by the phospholipids automatically lining up into two layers. The hydrophobic fatty acid tails of the molecules are located on the inside of the layers and act as an impenetrable wall to water-soluble molecules. Across the cell membrane boundary, there exists an electropotential gradient referred to as the membrane potential and measured on a scale of millivolts. The inside of the cell is negatively charged with respect to the outside.

Cells can be divided into two groups: excitable cells and nonexcitable cells. Excitable cells have the ability to generate action potentials, which are voltage-dependent inward ionic currents across the plasma membrane in response to a sufficient stimulus. In contrast, if a current is applied to a nonexcitable cell, the potential will instantaneously return to rest once the stimulus is removed. Both nerve cells and endocrine cells are excitable cells. The latter, in particular the $\beta$-cell, will be the focus of this thesis.

The composition of the cell membrane plays an important role in its electrophysiological dynamics. Many types of protein molecules can be found within the phospholipid bilayer. Some proteins are receptors for chemical signals or enzymes that catalyze reactions. Other proteins regulate the transport of ions across the cell membrane. These protein molecules form pores in the membrane called ionic channels.

An important finding from research on ionic channels is that they act as selective gates, only permitting a specific type of ion to pass through. Another finding is that the channels are not open at all times. Channels are regulated primarily by changes in voltage and ionic concentration. Other chemicals such as ATP (adenosine triphosphate) can affect the state of an ionic channel as well. If a channel is activated by a change in membrane potential it is said to be voltage-

gated. Changes in ionic concentrations, either inside or outside the cell, can also affect the status of an ionic channel. This type of channel is called ion-gated. The protein channels play a major role in electrical activity seen in different types of cells.

The concentration gradient present across the cell membrane is due to differences in concentration of ions inside and outside the cell. Potassium ions, for example, are at a higher concentration inside the cell than outside, while sodium, calcium and chloride ions are more abundant outside the cell relative to the inside.

Ionic movement through open channels is driven by differences in electric potential and ionic concentration across a cell membrane, as well as by the binding of ligands, or messenger molecules. For example, potassium ions are at a much higher concentration inside the cell, therefore the concentration gradient pushes potassium ions outward through open channels. In contrast, the electrical gradient tends to hold the positively charged $K^+$ ions inside the cell membrane since the inside is about -60 mV with respect to the outside. The net forces are in opposition and it is not immediately apparent which influence, diffusional or electrostatic, would have the greater influence. In order to compare the magnitude of these forces, the concentration gradient can be expressed as an equivalent electrical gradient, using the *Nernst equation*. The Nernst potential for a particular ion, $V_{ion}$ is as follows.

$$V_{ion} = \frac{RT}{FZ} log_e \frac{C_o}{C_i} \tag{1.1}$$

where,

$R$ = universal gas constant (8.31 joules/mol/K),

$F$ = Faraday's constant (96.487 coulombs/mmole),

$T$ = absolute temperature (K),

$Z$ = valence of the ion,

$C_o$ = concentration of the ion outside the cell,

$C_i$ = concentration of the ion inside the cell.

The potential difference calculated from the Nernst equation is referred to as the equilibrium potential for the ion. For the potassium ion, $V_k \approx -75$ mV. Thus, if the inside of the cell membrane was at $-75$ mV in relation to the outside, then the net diffusional and electrostatic forces would be balanced.

The flow of charged particles through the protein channels generates electrical currents affecting the membrane potential. For example, in the nerve cell, potassium ($K^+$) and sodium ($Na^+$) ions are responsible for action potentials, during which membrane potential is briefly reversed. Voltage depolarizes rapidly from the rest state of approximately $-60$ mV, reaches a peak, then undershoots before returning to rest, as in Figure 1.1.

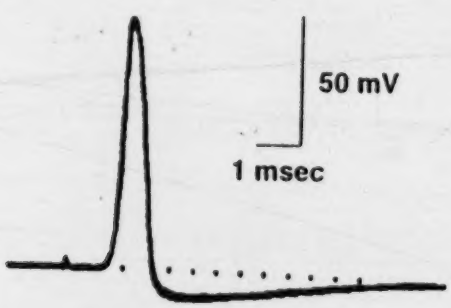


Figure 1.1: An action potential from the Hodgkin and Huxley neuron model, of a giant squid axon from [4].

In the next section, we will discuss a ground-breaking mathematical model of the membrane potential of a nerve cell. In Section 1.2, this model is then modified to describe the dynamics of $\beta$-cells.

### 1.1.1 Mathematical modelling of electrophysiological phenomena

The focus of this thesis will involve the electrophysiological behaviour of $\beta$-cells. The foundations for the basic mathematical model of the $\beta$-cell were laid by Hodgkin and Huxley [12] in their Nobel Prize winning work with neurons. Mathematical models of the nerve cell membrane can be used to understand how the membrane potential changes with the flow of ions. The technique lends itself nicely to $\beta$-cell models, as well as models of many other excitable cells.

Hodgkin and Huxley modelled the nerve cell membrane as a leaky capacitor, where current is passed through the membrane by the flow of ions or by charging the membrane capacity. Thus the total membrane current, $I_m$, is separated into capacitive current and ionic current, given by the following equation:

$$I_m = C_m \frac{dV}{dt} + I_i, \tag{1.2}$$

where $C_m$ denotes the membrane capacitance, $V$ is the membrane potential and $t$ represents time (with units: $1\mu\text{F/cm}^2$, mV, and msec respectively). $I_i$ represents the sum of all ionic currents.

Different currents flow through separate channels. Thus, under the assumption that all currents flow independently of each other, the total ionic current, $I_i$, is divided to illustrate the primary contributors, potassium and sodium ions, as well as a small leak current encompassing all other ions:

$$I_i = I_K + I_{Na} + I_l. \tag{1.3}$$

The difference between the concentration and electrical gradients for each ion produces a net driving force which is proportional to the difference between the membrane potential and the corresponding Nernst potential, $V - V_{ion}$. The ion carries a current which depends on this driving force as well as the permeability,

which is inversely proportional to resistance ($R$), of the membrane to the ion. Then according to Ohm's Law,

$$I_{ion} = g_{ion}(V - V_{ion}), \tag{1.4}$$

where the conductance, $g_{ion}$, replaces $1/R$ at the preference of physiologists. Therefore, for the potassium, sodium and leakage currents respectively we have,

$$I_K = g_K(V - V_K), \quad I_{Na} = g_{Na}(V - V_{Na}), \quad I_l = g_l(V - V_l).$$

By Kirchoff's Law, the capacitive and ionic currents are in balance, that is, the total membrane current ($I_m$) is zero. Therefore, incorporating the definitions above, equation (1.2) becomes

$$C_m \frac{dV}{dt} = -\left(g_K(V - V_K) + g_{Na}(V - V_{Na}) + g_l(V - V_l)\right). \tag{1.5}$$

The current balance equation is more complex than it appears due to the dynamic nature of the ionic conductances. The conductance, $g_{ion}$, is essentially the permeability of the membrane, or ease with which the ion passes through the membrane. Experimentally it has been observed that $g_{ion}$ depends on the state of the particular ionic channel, which depends on electrical and chemical gradients as well as binding of messenger molecules.

Hodgkin and Huxley thought of a channel as being composed of several gates, each of which is either opened or closed. Therefore, each conductance is a dynamic variable, depending on the status of the gates. For example, the potassium channel was assumed to be regulated by four equal gates, while the sodium channel was assumed to be regulated by three 'activation' gates and one 'inactivation' gate. The probability that a gate is open is represented by 'gating' variables, $h, m, n$, where $h$ is the variable representing the status of the inactivation gate of the $Na^+$ channel, and $m$ and $n$ are the variables representing the status of the activation gates of the $Na^+$ and $K^+$ channels respectively. Since $h, m$, and $n$

represent probabilities, their values range between 0 and 1. The individual ionic conductances are specified by the product of a maximal conductance, realized if all relevant channels are opened, and the product of the corresponding gating variables. For example, the potassium conductance is written as

$$g_K = \bar{g}_K n^4, \tag{1.6}$$

where $\bar{g}_K$ is the maximal conductance for the $K^+$ channel, and the sodium conductance is written as

$$g_{Na} = \bar{g}_{Na} m^3 h, \tag{1.7}$$

where $\bar{g}_{Na}$ is the maximal conductance for the sodium channel. The exponents to which the gating variables are raised were chosen by Hodgkin and Huxley based on a 'best fit' to available experimental data. However, several years after this work was completed, it was discovered that the $Na^+$ channel, for example, is formed by a single protein molecule consisting of four subunits, three of which are identical and one, distinct from these three. The $Na^+$ channel is assumed to be opened if three similar subunits ('particles') are active ('occupy certain positions') and one other subunit is inactive.

The dynamics of the gating variables, $h, m$, and $n$, are described by the following equation:

$$\frac{dx}{dt} = \alpha_x(V)(1-x) - \beta_x(V)x, \quad x = h, m, n. \tag{1.8}$$

where $\alpha_x(V)$ and $\beta_x(V)$ are rate constants. Consider the above equation for the gating variable $n$ of the $K^+$ channel. Interpreting the equation physically, we must assume the potassium ions can only cross the membrane if all four gates are open which occurs if four similar particles occupy a certain region of the membrane. Then $n$ represents the proportion of open gates, and $(1-n)$ is the proportion of closed gates. The rate at which closed gates open is given by $\alpha_n$, and the rate at which open gates close is $\beta_n$. The interpretation is similar for $m$ and the $Na^+$

channel. However, the sodium inactivation variable $h$, represents the proportion of closed gates, thus the directions of the rate constants are reversed.

The kinetics of the gating variables in (1.8) are more often expressed in the following equivalent form,

$$\frac{dx}{dt} = [x_\infty(V) - x]/\tau_x(V), \quad x = h, m, n, \tag{1.9}$$

where

$$x_\infty(V) = \alpha_x(V)/[\alpha_x(V) + \beta_x(V)],$$
$$\tau_x(V) = 1/[\alpha_x(V) + \beta_x(V)].$$

Fits for $x_\infty$ and $\tau_x$ for $x = h, m, n$ were obtained by Hodgkin and Huxley using experimental data. For details about the functional form and parameter values the reader is referred to [12]. In this format, the functions $\tau_x$ can be interpreted as time constant functions, and $x = x_\infty$ for $x = h, m, n$ can be interpreted as the steady-state functions. For example, if $V$ were suddenly moved to $V^*$ and held there, then $x \to x_\infty(V^*)$ with time constant $\tau_x(V^*)$. The steady-state functions for the activation variables, $m$ and $n$, increase with $V$, in contrast to $h_\infty$ which decreases with $V$, as illustrated in Figure 1.2.

The complete four dimensional system of equations as in (1.5)–(1.9) is as follows.

$$C_m \frac{dV}{dt} = -\left(\bar{g_K} n^4 (V - V_K) + \bar{g_{Na}} m^3 h (V - V_{Na}) + g_l (V - V_l)\right), \tag{1.10}$$

$$\frac{dn}{dt} = [n_\infty(V) - n]/\tau_n(V), \tag{1.11}$$

$$\frac{dm}{dt} = [m_\infty(V) - m]/\tau_m(V), \tag{1.12}$$

$$\frac{dh}{dt} = [h_\infty(V) - h]/\tau_h(V). \tag{1.13}$$

If the correct choice of model parameters is used, this system can produce a solution similar to Figure 1.1. This system provides a basis for future mathematical models of membrane electrical activity. In other excitable cells, such as the

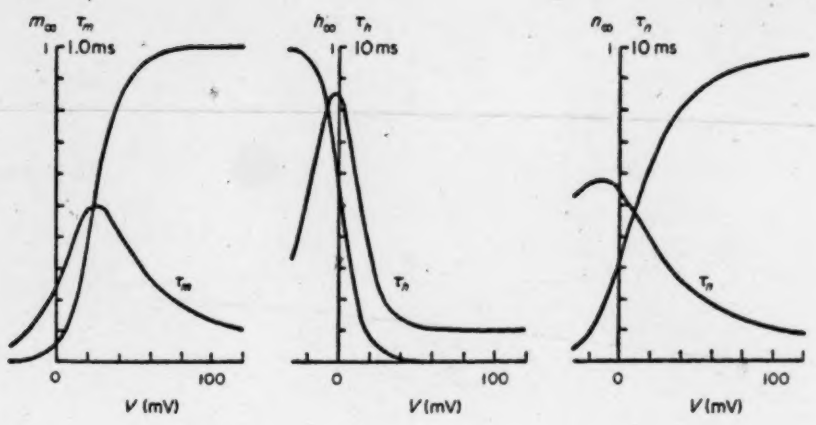


Figure 1.2: Steady state curves and time constant functions for $m$, $n$ and $h$ as functions of membrane potential from [22].

pancreatic $\beta$-cells, a similar modelling approach can be utilized, incorporating the particular ionic channels of the $\beta$-cell. These models will be the topic of the next section.

## 1.2 Electrophysiology of $\beta$-cells

We now turn our attention to $\beta$-cells, which are secretory cells, responsible for the secretion of insulin in response to stimulatory glucose levels. Insulin is the only hormone capable of lowering blood glucose concentrations. Therefore, defects in $\beta$-cell responsiveness can lead to metabolic disorders such as those associated with diabetes.

$\beta$-cells are clustered together and coupled to their nearest neighbours by low resistance electrical pathways in functional units called islets of Langerhans. In the human pancreas, there are on the order of one million of these roughly spherical structures, with a radius ranging from 50 to 250 $\mu$m. $\beta$-cells comprise about

$70 - 90\%$ of the islet. The diameter of a $\beta$-cell is approximately $10 - 15$ $\mu$m. About $100 - 200$ other secretory cells can also be found in an islet, including $\alpha, \delta$ and peptide cells. These cells are located mainly around the periphery, and secrete other substances such as glucagon.

As previously mentioned, endocrine cells, such as $\beta$-cells belong to the class of excitable cells. Excitability was first reported in pancreatic islet $\beta$-cells by Dean and Matthews [10]. As in nerve cells, electrical activity in the $\beta$-cells is a result of temporal changes in the permeability of the $\beta$-cell membrane to various ions. The most important ion channels in the $\beta$-cell are selective for potassium and calcium ions and are both voltage-gated and ion-gated. The characteristic pattern of electrical activity observed in $\beta$-cells alters between a silent phase, where the membrane potential changes very slowly, and a active phase during which the membrane potential oscillates rapidly, as depicted in Figure 1.3. This phenomenon is referred to as bursting. The plateau fraction is the ratio of the duration of the active phase to the period of the burst.

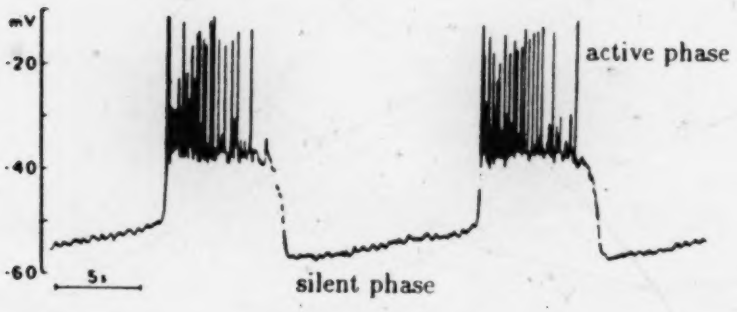


Figure 1.3: Bursting pattern induced by 10 mM glucose as observed in a mouse pancreatic $\beta$-cell.(Adapted from [17])

Bursting in $\beta$-cells differs from the bursting that is exhibited by many neurons in that the action potentials of the active phase do not undershoot the membrane potential of the silent phase. The repetitive firing phase begins at a depolarized plateau. Therefore, this pattern is sometimes called 'square-wave bursting'.

Bursting behaviour is induced by the introduction of glucose into the system. Addition of glucose at concentrations up to 5 mM results in only a gradual depolarization of the membrane potential from the usual steady state ($\approx -65$ mV) to a new steady-state level. Higher glucose concentrations cause the membrane to depolarize past the threshold of about $-55$ mV where bursting is initiated. Bursting serves to facilitate an influx of calcium into the $\beta$-cells. This results in a periodic increase in ionic calcium concentration which initiates a complex sequence of events eventually resulting in the secretion of insulin. In this way, electrical activity links the glucose signal and the response of insulin secretion.

### 1.2.1 Single $\beta$-cell model

The first mathematical model of bursting in $\beta$-cells was developed by Chay and Keizer [8], based on a hypothesis of Atwater and colleagues [2]. They adapted the model by Hodgkin and Huxley, discussed in Section 1.1.1, to incorporate the known channels of the $\beta$-cell membrane, and to permit bursting activity. The ionic channels included in the Chay-Keizer model included voltage-gated potassium and calcium channels, as well as calcium-activated potassium channels. In this model, the influx of calcium through the voltage-gated calcium channels during the active phase slowly increases the intracellular calcium concentration, $[Ca^{2+}]_i$. This slowly activates the calcium-activated potassium channels. The active phase is ended when the repolarizing drive caused by the calcium-activated potassium channels is sufficiently large. Then, during the silent phase, intracellular $Ca^{2+}$ ions are slowly removed from the cell by membrane pumps. This

deactivates the calcium-activated potassium channels and allows the repetitive firing stage to begin again. Therefore, it was originally predicted that the ionic calcium concentration was responsible for the slow alteration between active and silent phases, and therefore would oscillate on a slow time scale, accumulating slowly during the active phase then decreasing with the onset of the silent phase. This first attempt was remarkably successful at modelling the burst pattern and response to changes in glucose concentration. Unfortunately, when it became possible to image $[Ca^{2+}]_i$ during bursting, it was shown that $[Ca^{2+}]_i$ reaches a plateau almost simultaneously to the beginning of the active phase. Thus, it became the task of modellers to find another variable or variables that could cause the switch between active and silent phases.

Keizer and Magnus [14] proposed that the mechanism for bursting involves the ratio of cytoplasmic ATP (adenosine triphosphate) to ADP (adenosine diphosphate). When glucose enters a $\beta$-cell and is metabolized, ATP is synthesized from ADP. The increase in the ATP/ADP ratio decreases the conductance of the ATP-modulated potassium channels, $g_{K(ATP)}$, causing the cell to depolarize. Cellular depolarization opens the voltage-gated $Ca^{2+}$ channels which allows $Ca^{2+}$ to enter, further depolarizing the cell and initiating excitable behaviour such as bursting. As glucose is used, the production of ATP decreases, reducing the ATP/ADP ratio and increasing the K(ATP) conductance. As the K(ATP) channels open, $K^+$ ions flow out of the $\beta$-cells which decreases or repolarizes the membrane potential and terminates the active phase. In this way, the slowly oscillating ATP/ADP ratio was considered to cause the transition between active and silent phases of bursting electrical activity. Another possibility for the slow process could be the voltage-dependent inactivation of an excitatory $Ca^{2+}$ current [28]. However, thus far none of the proposed mechanisms for bursting have been able to measure up to stringent experimental verification [23].

Regardless of the hypothesized slow process underlying bursting, all the models of $\beta$-cell electrical activity are based on the same premise, namely bistability of the cell membrane. The cell either is at a stable hyperpolarized membrane potential (silent phase), or in a depolarized spiking state (active phase). The slow process is responsible for switching the cell between these two states.

Due to the uncertainty regarding the identity of the slow variable(s), Sherman and Rinzel [26] introduced the use of an abstract slow variable, $S$, acting through a slow current $I_S$. Here the slow variable is assumed to activate a voltage-independent $K^+$ conductance. They use a simplified biophysical model in order to derive general results with a broad range of applications. We explain the mechanism of bursting with this generic model describing the dynamics of a single $\beta$-cell which is assumed to be part of a perfectly synchronized islet. The nondimensionalized system of ordinary differential equations is:

$$\tau \frac{dV}{dt} = -I_{Ca}(V) - I_K(V,n) - I_S(V,S), \tag{1.14}$$

$$\tau \frac{dn}{dt} = \lambda(n_\infty(V) - n), \tag{1.15}$$

$$\tau_S \frac{dS}{dt} = S_\infty(V) - S, \tag{1.16}$$

where the calcium, potassium and 'slow' currents are given respectively by,

$$I_{Ca} = g_{Ca} m_\infty(V)(V - V_{Ca}), \quad I_K = g_K n(V - V_K), \quad I_S = g_S S(V - V_K), \tag{1.17}$$

where

$$x_\infty(V) = \frac{1}{1 + exp((V_x - V)/\theta_x)}, \quad \text{for } x = m, n, S. \tag{1.18}$$

This model has been greatly simplified from the model by Hodgkin and Huxley in section 1.1.1. The $Na^+$ contribution to the current balance equation has been replaced by the $Ca^{2+}$ current to reflect $\beta$-cell physiology. The inactivation variable $h$ has been completely eliminated, and the $Ca^{2+}$ activation variable $m$ is assumed

to act instantaneously and therefore is replaced by its steady state value $m_\infty$. As well, the exponents for all the gating variables have been removed. In addition, the voltage dependence of the time constants, $\tau$ and $\tau_S$, has been eliminated. The two independent time constants have the relationship $\tau << \tau_S$, which is critical for the dynamics of the system as the slow wave and fast spike generating mechanisms must operate on different time scales. The spikes during the active phase are due to the $Ca^{2+}$ and $K^+$ currents as given by the equations for $V$ and $n$. During the active phase, $S$ slowly accumulates. This causes the membrane potential to become less excitable by raising the threshold for bursting. The spike minima, at the base of the plateau, also hyperpolarize. As the threshold and spike minima come together, the burst ends.

A typical bursting solution for the model generated by XPP [10] is illustrated in Figure 1.4, accompanied by the corresponding slow oscillation in the variable $S$. The parameter values used can be found in Table 1.1.

| Symbol | Value | Symbol | Value |
|---|---|---|---|
| $g_{Ca}$ | 3.6 | $\theta_m$ | 12 mV |
| $g_K$ | 10 | $V_m$ | -20 mV |
| $g_S$ | 4 | $\theta_n$ | 5.6 mV |
| $\tau$ | 20 msec | $V_n$ | $-17$ mV |
| $\tau_S$ | 35000 msec | $\theta_S$ | 10 mV |
| $V_{Ca}$ | 25 mV | $V_S$ | $-38$ mV |
| $V_k$ | $-75$ mV | $\lambda$ | 0.9 |

Table 1.1: Parameter values for the single $\beta$-cell model.

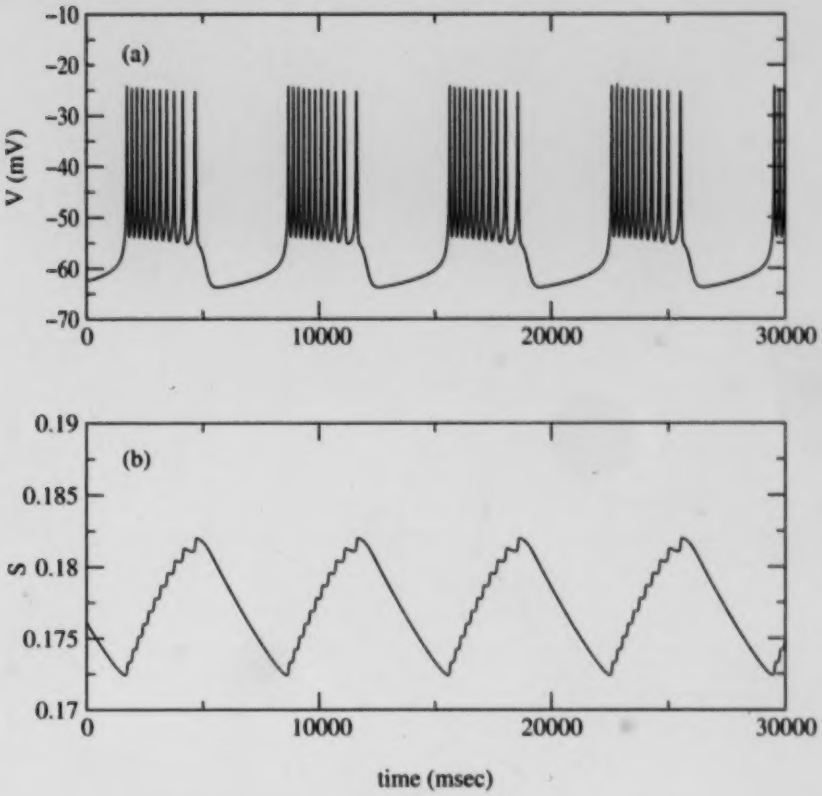


Figure 1.4: (a) Characteristic bursting pattern of the $\beta$-cell, (b) Dynamics of the slow variable $S$ during the bursting in (a).

### 1.2.2 Electrophysiological effects of glucose

Glucose-stimulated insulin secretion is of great importance in the maintenance of glucose homeostasis. Defects in this process are a critical component of type II diabetes, and this motivates further study. Recall that glucose metabolism causes a rise in the ratio of ATP to ADP, resulting in the closure of K(ATP) channels, and eventually the influx of $Ca^{2+}$. The best biophysical candidate for an electrical glucose sensor is the K(ATP) conductance, $g_{K(ATP)}$ [24], since closure

of K(ATP) channels implies a decrease in $g_{K(ATP)}$. Therefore, increased glucose corresponds to a decrease in $g_{K(ATP)}$. Thus, the K(ATP) channel provides a connection between glucose metabolism and $Ca^{2+}$ influx, necessary for insulin secretion.

In the absence of glucose ($G$), a $\beta$-cell would be essentially quiescent. Increasing $G$ towards 5 mM causes the membrane potential to depolarize. Additional glucose stimulation initiates bursting electrical activity, and as $G$ increases so does the plateau fraction. The plateau fraction increases gradually until it reaches 1, or continuous spiking, when the islet is exposed to a very high glucose concentration ($> 20$ mM) [24].

In order to incorporate glucose sensing into the generic model stated above, we must include the contribution of the K(ATP) channel in the current balance equation (1.14) which becomes

$$\tau \frac{dV}{dt} = -I_{Ca}(V) - I_K(V,n) - I_S(V,S) - I_{K(ATP)}(V), \tag{1.19}$$

where $I_{K(ATP)}(V) = \bar{g}_{K(ATP)}(R - 0.5)(V - V_K)$, and the other currents are unchanged. The maximal K(ATP) conductance is multiplied by a factor of $(R-0.5)$, where $R$ is the glucose sensing parameter. Decreasing $R$ is interpreted as an increase in glucose. Changes in $R$, or similarly $G$, only affect the plateau fraction as illustrated in Figure 1.5. Relatively small changes in $R$ result in substantial changes in the plateau fraction, from a plateau fraction of about $1/6$ for $R = 0.8$ to a plateau fraction of 1, corresponding to continuous spiking, for $R = 0.3$.

It is apparent that changes in glucose, represented by changes in $R$, have a profound effect on $\beta$-cell electrical activity. In the next section, we will consider, in detail, the process of glucose diffusion into an islet.

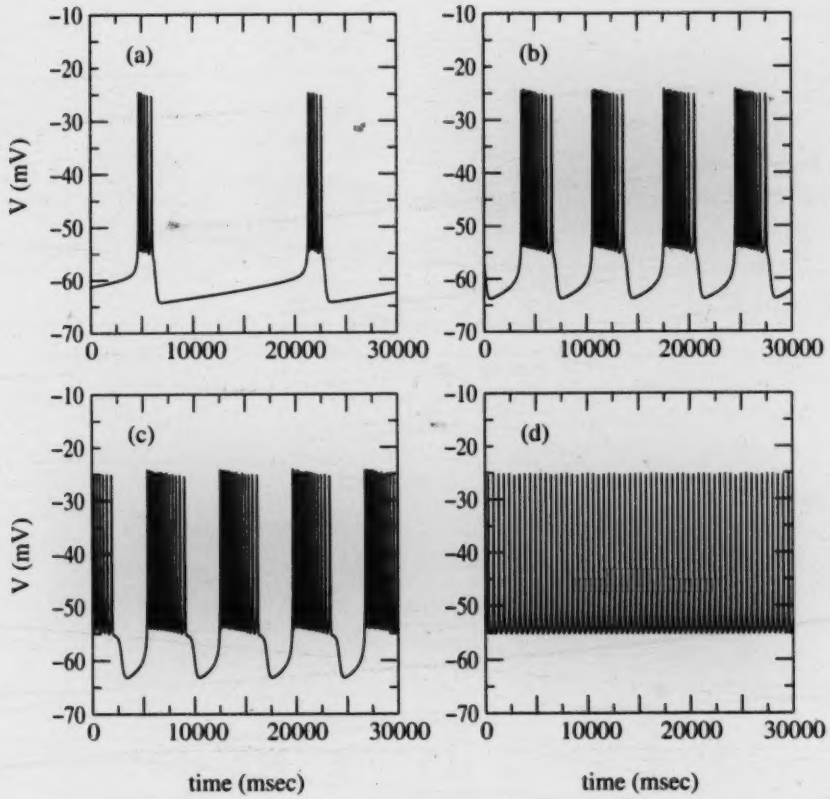


Figure 1.5: Bursting of the membrane potential for the following values of the glucose sensing parameter. A decrease in $R$ corresponds to an increase in glucose. (a) $R = 0.8$ (b) $R = 0.5$ (c) $R = 0.4$ (d) $R = 0.3$.

## 1.3 Glucose diffusion

In experimental studies, an islet of Langerhans is secured to the bottom of a perifusion chamber. Through an inflow tube, substances such as glucose are introduced to the bath and the electrophysiological response of the $\beta$-cells inside the islet is continuously observed. A common experimental protocol is to study the response of an islet to step changes in glucose concentration, where the glucose bath is refreshed continually to keep it at a constant level. As glucose diffuses into the islet, the electrically excitable $\beta$-cells inside depolarize, initiating bursting electrical activity when the glucose concentration reaches a certain threshold.

When an isolated islet is exposed to a stimulatory concentration of glucose there is a 1-2 minute delay before islet electrical activity begins [27]. In [6], Bertram and Pernarowski hypothesize that this delay is due in part to the delay in penetration of glucose into the inner portions of the islet. Bertram and Pernarowski test this hypothesis by formulating a model of hindered glucose diffusion. We review their work here.

The main focus of their study was to determine the glucose distribution in the islet after exposure to a stimulatory concentration of glucose at a time when islet electrical activity is likely present. For a relatively small islet of radius 100 $\mu$m and a bath glucose concentration of 10 mM, it was found the islet was not near a uniform glucose distribution 2 minutes after the bath was applied, when electrical activity is usually occurring. In fact, near the center of the islet, glucose concentration in the $\beta$-cells was less than 5 mM. It has been documented that isolated $\beta$-cells exposed to a glucose concentration of 7 mM or more will become electrically active [3]. However, even for high values of porosity and permeability used in the numerical approximations, only the cells near the periphery of the islet would have been exposed to sufficient glucose to become active and the cells near the center would be silent. These results indicate that the synchronized electrical

activity observed in islets occurs when only some of the cells are exposed to a stimulatory glucose level. The cells on the periphery that become electrically active recruit the cells with sub-stimulatory glucose levels, and the islet bursts in synchrony.

In the model developed to simulate the diffusion process, a simplifying assumption is made that the islet is made up entirely of $\beta$-cells. This is a reasonable assumption when considering that there are $1000 - 10000$ $\beta$-cells in a single islet and only $100 - 200$ other secretory cells. Glucose diffusion through the islet is affected by several factors. It is assumed that glucose diffuses mainly through the space between cells. This property is incorporated through the use of an 'effective' diffusion rate taking into account the porosity of the islet. Therefore, if the islet is very crowded with cells, or less porous, diffusion will be hindered, which is reflected in a decreased rate of diffusion. Glucose diffusion is also hampered by a thick layer of cells, called the acinar layer, surrounding the islet. The permeability of this layer is incorporated into the model and the effects of varying the permeability are investigated.

As glucose penetrates through the acinar layer into the islet and contacts the $\beta$-cells, some glucose is transported into the $\beta$-cells by a GLUT-2 transporter. This slows down the penetration of glucose into the islet. Using transport rate values obtained experimentally [13], the effect of GLUT-2 transporters on glucose diffusion is incorporated into the model, assuming transport is uniform throughout the islet. Analysis of the model showed the strong impact on diffusion made by the transportation of glucose into the $\beta$-cells. In a simulated islet of radius 200 $\mu$m exposed to a glucose bath of 10 mM, approximately 5 minutes were required for the center of the islet to reach 90 % of the bath concentration when GLUT-2 transport is included. However, in absence of transport, glucose would reach 90 % of the bath concentration at the center after only 1 minute.

Once glucose has been transported inside a $\beta$-cell, a domino effect occurs that initiates electrical activity. First, the glucose is metabolized to produce ATP, increasing the ratio of ATP to ADP. The increase in ATP inactivates the K(ATP) channels in the cell membrane and the cell becomes depolarized. The time it takes for glucose to be metabolized may also contribute to the 1-2 minute delay observed between exposure of an islet to stimulatory glucose bath and the beginning of electrical activity. However, metabolism of glucose by the $\beta$-cells is not incorporated into the model since experimental results have indicated that the glucose concentration within a $\beta$-cell equilibrates very quickly to a concentration slightly lower than the concentration outside the cell [30].

Gap junctions that electrically couple $\beta$-cells tend to synchronize electrical activity throughout the islet. Therefore, as glucose diffuses into the islet, cells on the periphery are stimulated to become eletrically active. However, these cells may be restrained by the majority of cells in the interior that still remain inactive. This implies that the entire islet will not exhibit synchronized electrical activity, or bursts, until the glucose has diffused into the islet sufficiently far to activate sufficiently many $\beta$-cells. The exact ratio of active to silent cells necessary for the islet to begin bursting is not known. This supports the hypothesis that the delay described can be, at least in part, attributed to the time it takes for glucose to diffuse into the islet.

The glucose in the extracellular space, between the $\beta$-cells, is referred to as extracellular glucose, with its concentration denoted by $g_e$. The glucose concentration within the $\beta$-cells, or intracellular glucose concentration, is given by $g_i$. In an islet of radius $a$, the glucose diffusion process is modelled in spherical coordinates and assuming spherical symmetry. The partial differential equation describing the behaviour of $g_e$ is

$$\frac{\partial g_e}{\partial t} = pD_G \frac{1}{r^2}\frac{\partial}{\partial r}\left(r^2 \frac{\partial g_e}{\partial r}\right) - \frac{1}{\rho}F(g_e, g_i), \quad r < a, \quad t > 0. \tag{1.20}$$

The 'effective' glucose diffusion, as discussed above, is given by the product of the porosity $p \in [0,1]$ and the diffusion coefficient of glucose in water $D_G$. The GLUT-2 transport mechanism, represented by the function $F(g_e, g_i)$, depends on both the extracellular glucose concentration ($g_e$) and the glucose concentration within the $\beta$-cells ($g_i$). The precise form of the transport function will be specified later. The number of $\beta$-cells in the islet will affect the amount of glucose transported from extracellular space inside the $\beta$-cells. This is reflected in the model by the parameter $\rho = V_e/V_i$, the volume fraction of total volume of extracellular space ($V_e$) to total $\beta$-cell volume ($V_i$). Studies [7] have shown that the extracellular volume is only 1-2 % of the total islet volume, so $\rho = 0.02$ is used for the volume fraction. In the model, the inverse of the volume fraction accurately reflects the property that an increase in $\beta$-cell volume ($V_i$) would result in further reduction of extracellular glucose due to GLUT-2 transport, and therefore diffusion would be slowed.

Initially, the glucose concentration in the islet is assumed to be zero, i.e.,

$$g_e(r,0) = 0, \quad r \in [0,a]. \tag{1.21}$$

Boundary conditions are obtained by assuming that the acinar layer is a passive membrane. Therefore, the chemical gradient across the surrounding layer is the only source of flux. If the glucose bath concentration is given by $G_{bath}$, and the permeability of the acinar layer given by $k$, then an appropriate boundary condition is

$$\frac{\partial g_e}{\partial r} = k(G_{bath} - g_e), \quad r = a, \quad k > 0. \tag{1.22}$$

In addition, the glucose concentration at the center of the islet is assumed to be bounded:

$$|g_e(0,t)| \leq M < \infty, \quad t \geq 0. \tag{1.23}$$

The dynamics of the intracellular glucose concentration, $g_i$, are modelled by assuming that glucose enters the $\beta$-cells only via GLUT-2 transport. No diffusion

through gap junctions is considered, although there is some evidence that this is possible [20]. The following differential equation results:

$$\frac{\partial g_i}{\partial t} = F(g_e, g_i). \tag{1.24}$$

Taking the initial glucose concentration inside the $\beta$-cells to be zero, we have

$$g_i(r, 0) = 0, \quad r \in [0, a]. \tag{1.25}$$

The derivation of the GLUT-2 transport function $F(g_e, g_i)$ is complex and the motivation will not be discussed in detail here. For full details the reader is referred to [6]. A process of facilitated diffusion allows glucose molecules to pass across the $\beta$-cell membrane. The maximum transport rate is given by $V_{max}$ and $K_m$ is the transporter dissociation constant. The glucose flux into the cell is represented by

$$F(g_e, g_i) = R_{max} \frac{(g_e - g_i)K_m}{(K_m + g_e)(K_m + g_i)}. \tag{1.26}$$

Values for the parameters in the model given by equations (1.20)–(1.26) are given in Table 1.2.

| Symbol | Description | Value |
|---|---|---|
| $D_G$ | Glucose diffusivity in water | $0.673 \times 10^{-5}$ cm$^2$ |
| $a$ | Islet radius | 100 $\mu$m |
| $\rho$ | Volume fraction | 0.02 |
| $R_{max}$ | GLUT-2 maximum uptake rate | 0.52 mM/s |
| $K_m$ | GLUT-2 dissociation constant | 17 mM |
| $k$ | Acinar layer permeability | $0.2 - 1.0$ $\mu$m$^{-1}$ |
| $p$ | Islet porosity | $0.2 - 1.0$ |

Table 1.2: Parameter values for the glucose diffusion model [6].

Before analyzing the coupled, nonlinear system given by (1.20)–(1.26), the variable transformations $\tilde{g}_e = g_e r$ and $\tilde{g}_i = g_i r$ are applied to deal with the

singularity of (1.20) at the islet center. Numerical solutions were calculated using the software package XTC [?], using an implicit backwards Euler method with $\Delta t = 0.1$ s and $\Delta r = 2$ $\mu$m and an islet radius of $a = 100$ $\mu$m.

For the porosity and permeability values used ($p = 0.3, k = 0.3$ $\mu m^{-1}$) and a glucose bath concentration of 10 mM, it was found that the glucose distribution in the islet is far from equilibrated 2 minutes after the glucose bath is introduced. The extracellular and intracellular glucose concentrations are plotted at various times in Figure 1.6. However, islet electrical activity is typically observed approximately 2 minutes after a stimulatory glucose bath is in place. Therefore, this would indicate that electrical activity is occurring long before the glucose concentration inside the islet has reached a relatively even distribution.

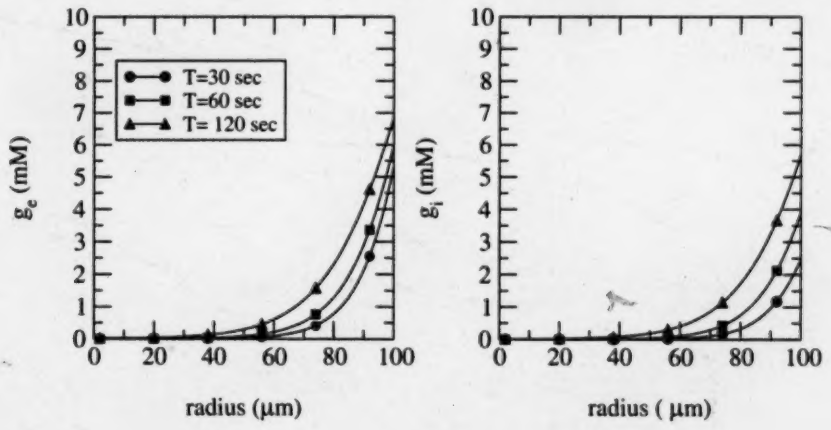


Figure 1.6: Extracellular ($g_e$) and intracellular ($g_i$) glucose concentrations in the islet 30 seconds, 1 minute, and 2 minutes after exposure to a 10 mM glucose bath. Computations were made using permeability and porosity values of $k = 0.1$ $\mu m^{-1}$ and $p = 0.1$ respectively, other parameter values are as in Table 1.2.

For values of islet porosity ranging from 0.1 to 1.0, and a similar range of permeability values, the glucose concentration near the center of the islet is cal-

culated numerically 2 minutes after the bath application of 10 mM glucose. It is shown that the concentration of glucose in the interior of the islet, in each case, is far from the bath concentration. In particular, the glucose concentration inside the $\beta$-cells ($g_i$) at a radius of 2 $\mu m$ after two minutes does not even reach 5 mM, half the bath concentration, for unrealistically high values of porosity and permeability ($k = 1.0\ \mu\text{m}^{-1}$, $p = 1.0$).

Also illustrated by these calculations is the major impact of an increase of islet porosity on $g_i$. The impact of increasing the permeability of the acinar layer is not as strong however, and for $k \geq 0.1\ \mu\text{m}^{-1}$, $g_i$ stays roughly the same. These properties are consistent with the results obtained when considering the values of $p$ and $k$ in the model in the absence of glucose transport.

In [6], it is proposed that the time required for glucose to equilibrate throughout the islet is on the order of several minutes, long after electrical activity is likely to have begun inside the $\beta$-cells of the islet. These findings provide the primary motivation for further study of the effect of glucose diffusion on the electrical activity of $\beta$-cells within an islet.

## 1.4 Thesis outline

In order to get a 'big picture' of islet eletrophysiological dynamics, we propose to merge the model of hindered glucose diffusion by Bertram and Pernarowski with a generic model of islet electrical activity. In Chapter 2, a model is developed to simulate the initiation of electrical activity in an islet after exposure to a stimulatory glucose concentration. This combined model is developed in two steps. First, a three-dimensional islet model is obtained by extending the single cell model discussed in Section 1.2.1. This is done by incorporating gap junctional coupling of $\beta$-cells and implementing the theories presented by Pernarowski in [19]. Next, the islet model is connected to the model of glucose diffusion described in the

introductory Section 1.3, through an expression that accounts for the known effects of glucose on electrical activity in $\beta$-cells. The complete combined model is described as well as the numerical methods used to solve the resulting system of partial differential equations.

In Chapter 3, the combined model will be used to test the hypothesis proposed in [6], that the delay in islet electrical activity is due in part to the time required for glucose to diffuse into the islet. The results of Bertram and Pernarowski [6] indicate that electrical activity begins long before glucose is equilibrated throughout the islet. We show that this is indeed the case. In this chapter, we also investigate what fraction of the islet must be exposed to a stimulatory glucose concentration in order to initiate bursting electrical activity. In addition, the model will be used to study the emergence of synchronized islet electrical activity, considering such issues as; how the islet electrical activity can synchronize in the presence of a glucose gradient. We also consider variations in the glucose bath concentration and coupling strength, and possible effects on the delay in the onset of electrical activity in the islet. The delay is quantified as a function of the pertinent model parameters.

Finally, in Chapter 4, we present a general discussion of the ideas and models developed in this thesis. In addition, we consider possible modifications to the combined model and suggest experiments that might be performed.

# Chapter 2

# Development of the Combined Model

The single $\beta$-cell model discussed in 1.2.1 describes the behaviour of one cell as part of a synchronized functional unit or islet. Synchronization of electrical activity in an islet is most likely due to gap junction coupling, but some doubt remains as to whether coupling is strong enough and widespread enough [18]. In this chapter, we will extend the single $\beta$-cell model of Section 1.2.1 to a model of an islet. This will be done by incorporating the role of gap junctions in islet electrical activity.

In Section 2.1, we will describe a three dimensional discrete islet model, in which the islet is represented by an array of possibly hundreds of cells. In Section 2.2, gap junctional coupling in the discrete model is replaced by a diffusion term and a continuum (partial differential equation) model results. A means of connecting the glucose concentration in the islet to the model of islet electrical activity will be introduced in Section 2.3. Finally, in Section 2.4 the complete combined model will be described, and the numerical methods used to solve the system are discussed in Section 2.5.

## 2.1 Discrete gap junctional coupling

It has been shown [17] that $\beta$-cells are electrically coupled together by gap junctions. Gap junctions are formed by protein molecules in the cell membrane. The protein pores make an electrical connection between most adjacent cells. Electrical recordings of $\beta$-cell pairs extracted from an islet indicated that 65% of cell pairs were electrically coupled, and the coupling conductance ($g_c$) was measured at $215 \pm 110$ pS [17]. In the nondimensional model used in this thesis, $g_c << 1$ implies weak coupling, $g_c \approx 1$ is intermediate coupling, and $g_c >> 1$ implies very strong coupling. It is believed that islets depend on gap junctions to produce a coordinated electrical response to glucose stimulation.

Coupling has effects on $\beta$-cell electrical activity other than aiding in synchronization. For example, Sherman and Rinzel [25] have shown that the length of time the cells spend bursting is maximized for an intermediate coupling strength. When cells are coupled and the coupling is strong enough to synchronize the bursts but not the spikes, the spikes are out of phase which causes their potentials to be pulled together. This reduces the spike amplitude and raises the spike plateau. Therefore, the slow variable must increase further to end the burst, thereby increasing the burst period. An increased burst period, or higher plateau fraction, results in an increase in the average $[Ca^{2+}]_i$, which translates to an increase in insulin secretion [11]. In addition, gap junctional coupling has been shown to aid in stabilizing the effects of noise and parameter variability on electrical activity patterns in islets [29]. Bursting is rarely observed experimentally in single $\beta$-cells, and much more often seen in sufficiently large, sufficiently tightly coupled clusters of cells. A typical islet burst ranges from $10 - 30$ sec, depending on the concentration of glucose to which the islet is exposed. In contrast, single cells tend to burst on a much longer scale of up to several minutes, or they burst much faster [15]. It is not clear which properties of islet electrical behaviour are

inherent to isolated cells or emergent features of coupling. However, it is well documented that electrical coupling between cells exists. Therefore, it is important to examine the behaviour coupled $\beta$-cells in an islet model.

Gap junctions are modelled as discrete diffusion of voltage, with voltage-independent conductances between pairs of cells. The current through gap junctions electrically connecting cells $i$ and $j$ is given by

$$I_{i,j} = g_{i,j}(V_i - V_j),$$

where $V_k$ is the membrane potential for cell $k$. The net conductance between cells $i$ and $j$ is given by $g_{i,j}$. For simplicity, it is assumed that the coupling conductance between cells is constant, i.e., $g_{i,j} = g_c$ for all $i, j$. Therefore, the total coupling current influencing the $i$th cell is obtained by taking the sum of all the coupling currents for each cell $j$ connected to the $i$th cell. We choose to model the islet as a three-dimensional rectangular array. Thus, all interior cells are coupled to 6 neighbouring cells, with corner, edge, and surface cells coupled to 3, 4, and 5 cells, respectfully. Let the $i$th $\beta$-cell be coupled to cells $\Omega_j$ with $j$ from 1 to M, where $M = 3$, 4, 5 or 6. Then for the $i$th cell, (1.14)-(1.19) becomes

$$\tau \frac{dV_i}{dt} = -I_{ion}(V_i, n_i, S_i) - \sum_{j=1}^{M} g_c(V_i - V_j), \tag{2.1}$$

$$\tau \frac{dn_i}{dt} = \lambda(n_\infty(V_i) - n_i), \tag{2.2}$$

$$\tau_S \frac{dS_i}{dt} = S_\infty(V_i) - S_i, \tag{2.3}$$

where $V_i, n_i$ and $S_i$ are membrane potential, gating variable and slow variable for the $i$th cell, and $I_{ion}$ represents the sum of all relevant ionic currents as described in (1.19), i.e.,

$$I_{ion} = -I_{Ca}(V_i) - I_K(V_i, n_i) - I_S(V_i, S_i) - I_{K(ATP)}(V_i, R).$$

This model works well for very small islets. However, for larger islets comprised of thousands of cells, computations take unreasonably long. We discuss a possible solution to this problem in the next section.

## 2.2 Continuum model

In [19], Pernarowski introduces a continuum model for islet electrical activity. First, a linear string of cells coupled by gap junctions is considered. If cell $i$ is located at $x_i = i\Delta x$, where $\Delta x$ is the $\beta$-cell diameter, then the coupling current ($I_c$) affecting cell $i$ would be given by the sum of the contributions from the cells to the left and right as follows

$$I_c = g_c(V_{i+1} - V_i) + g_c(V_{i-1} - V_i) = g_c(V_{i+1} - 2V_i + V_{i-1}).$$

The coupling current as expressed above can be seen to be a discretization of a diffusion term by letting

$$g_c = \frac{D}{\Delta x^2}, \tag{2.4}$$

which implies,

$$D\frac{\partial^2 V}{\partial x^2} \simeq \frac{D}{\Delta x^2}(V_{i+1} - 2V_i + V_{i-1}).$$

Therefore, in the continuum limit for a cell located at $x_i \in \mathbb{R}^3$, and homogeneous nearest neighbour gap junction coupling we have,

$$(D\nabla^2 V)|_{x=x_i} \simeq \sum_{j=1}^{M} g_c(V_j - V_i) = -\sum_{j=1}^{M} g_c(V_i - V_j). \tag{2.5}$$

The coupling current in (2.1) can then be replaced with the approximation above. Assuming spherical symmetry, the continuum model results from the approximation of (2.1)–(2.3) and is described by the following three-dimensional system of

partial differential equations in spherical coordinates:

$$\tau \frac{\partial V}{\partial t} = -I_{ion}(V, n, S) + D\left(\frac{\partial^2 V}{\partial r^2} + \frac{2}{r}\frac{\partial V}{\partial r}\right), \tag{2.6}$$

$$\tau \frac{\partial n}{\partial t} = \lambda\left(n_\infty(V) - n\right), \tag{2.7}$$

$$\tau_S \frac{\partial S}{\partial t} = S_\infty(V) - S. \tag{2.8}$$

Since cells on the boundary of the islet are not connected by gap junctions to any cells outside the cluster, there will be no current across the boundary. Hence, for the boundary given by $\partial\Omega$, the appropriate boundary condition is:

$$\nabla V \cdot \hat{N} = \frac{\partial V}{\partial n} = 0, \quad x \in \partial\Omega. \tag{2.9}$$

The initial conditions used are:

$$V(r,0) = -63.0 \text{ mV}, \qquad n(r,0) = 0.000268, \qquad , S(r,0) = 0.1027.$$

## 2.3 Development of the connection between the islet electrical activity model and the model of glucose diffusion

Before the process of glucose diffusion can be merged with the islet continuum model, as given by equations (2.6)–(2.9), the islet model must be altered so that it can reflect changes in glucose. In Section 1.2.2, the dependence of the $\beta$-cell electrical activity on glucose was modelled through the conductance of the ATP-regulated potassium channel via the 'glucose sensing' parameter $R$. Values of $R$ close to 1 corresponded to a low glucose concentration, and values of $R$ close to 0 reflected a high glucose concentration.

We assume that $R$ is related to the glucose concentration, $G$, via a sigmoidal relationship,

$$R(G) = c_1 \left( \frac{n^m}{n^m + G^m} \right) - c_2. \tag{2.10}$$

We fit (2.10) loosely to experimental data of Atwater and colleagues [1], which shows an increase in the plateau fraction for higher levels of glucose.

However, the response of a single cell to changes in $R$ is different from the response of a collection of cells coupled by gap junctions. In obtaining the relationship, we chose to use intermediate gap junctional conductance, $g_c$=1, which implies $D$ =100 pS $\mu$m$^2$ from (2.4). Experimental data indicates that gap junctional connections between $\beta$-cells have a mean conductance of between about 100 and 330 pS [17]. The nondimensional conductance $g_c$=1 falls within this range. The function $R(G)$ is calibrated to correspond to an islet of radius 100 $\mu$m, and the parameters $c_1, c_2, m$, and $n$ were chosen to be 2, 1.125, 3 and 16 respectively. A plot of the function $R(G)$ is given in Figure 2.1.

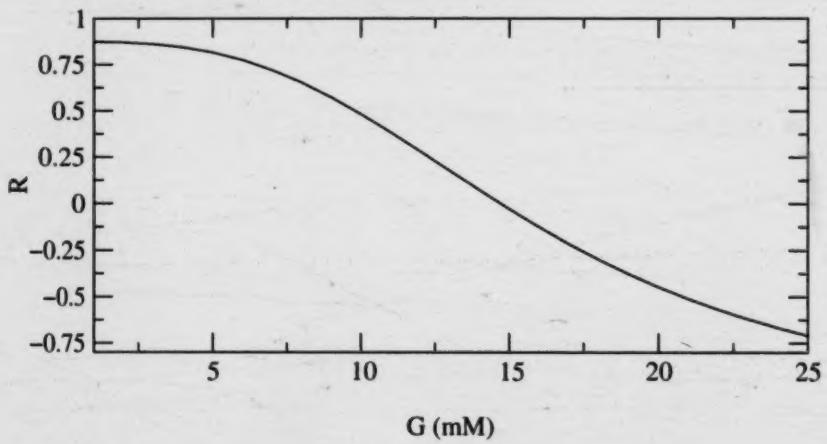


Figure 2.1: Plot of the function $R(G)$. As glucose increases $R$, and hence $g_{K(ATP)}$, decreases.

The K(ATP) current can now be expressed as a function of membrane poten-

tial and glucose concentration as follows,

$$I_{K(ATP)}(V,G) = \bar{g}_{K(ATP)}\left(c_1\left(\frac{n^m}{n^m+G^m}\right)-c_2\right)(V-V_K). \tag{2.11}$$

This equation is then substituted into the current balance equation (2.6). Finally, the glucose diffusion process can be combined with the islet continuum model.

## 2.4 Combined model

In this section, we incorporate the glucose diffusion model in the model for islet electrical activity. In (2.11), $G$ refers to glucose concentration local to the cell. Recall that the model for glucose diffusion involves both intracellular glucose ($g_i$) and extracellular glucose ($g_e$). When the glucose bath is first introduced, Bertram and Pernarowski [6] show that $g_i$ is significantly lower than $g_e$, but after several minutes the internal and exteral concentrations are essentially the same. Initially, we have chosen to use $g_e$ in the combined model, to most accurately reflect the experimental situation in which the glucose bath concentration ($G_{bath}$) is varied. The intracellular glucose concentrations are not generally measured. Therefore, $g_e$ will replace $G$ in the K(ATP) current (2.11).

To summarize, the combined model is described by the following set of partial differential equations from (2.6)–(2.11) and (1.20)–(1.26)

$$\tau\frac{\partial V}{\partial t} = -I_{Ca}(V)-I_K(V,n)-I_S(V,S)-I_{K(ATP)}(V,g_e)+D\left(\frac{\partial^2 V}{\partial r^2}+\frac{2}{r}\frac{\partial V}{\partial r}\right) \tag{2.12}$$

$$\tau\frac{\partial n}{\partial t} = \lambda\left(n_\infty(V)-n\right), \tag{2.13}$$

$$\tau_S\frac{\partial S}{\partial t} = S_\infty(V)-S, \tag{2.14}$$

$$\frac{\partial g_e}{\partial t} = pD\left(\frac{\partial^2 g_e}{\partial r^2}+\frac{2}{r}\frac{\partial g_e}{\partial r}\right)-\frac{1}{\rho}F(g_e,g_i), \tag{2.15}$$

$$\frac{\partial g_i}{\partial t} = F(g_e,g_i), \tag{2.16}$$

where the currents are given by

$$I_{Ca} = g_{Ca} m_\infty(V)(V - V_{Ca}),$$

$$I_K = g_K n(V - V_K),$$

$$I_S = g_S S(V - V_K),$$

$$I_{K(ATP)}(V, g_e) = \bar{g}_{K(ATP)} \left( c_1 \left( \frac{n^m}{n^m + g_e^m} \right) - c_2 \right) (V - V_K),$$

from equations (1.17) and (2.11), and the steady state activation and inactivation functions are given by

$$x_\infty(V) = \frac{1}{1 + exp((V_x - V)/\theta_x)}, \quad \text{for } x = m, n, S,$$

from (1.18), and the glucose transport function by

$$F(g_e, g_i) = R_{max} \frac{(g_e - g_i)K_m}{(K_m + g_e)(K_m + g_i)},$$

from (1.26). The boundary conditions are as previously described in Section 1.3 and Section 2.2, and all of parameter values are given in Table 2.1.

Computing solutions to the system is not completely straightforward due to the singularities introduced by the terms involving $1/r$ in the equations for both $V$ and $g_e$, (2.12) and (2.15) respectively. Therefore a transformation of variables is applied to eliminate these singularites, $\bar{V} = Vr$, $\bar{g}_e = g_e r$, and $\bar{g}_i = g_i r$. The numerical methods used to solve the resulting system for variables $\bar{V}$, $n$, $S$, $\bar{g}_e$, and $\bar{g}_i$, are discussed in detail in the next section.

## 2.5 Numerical methods

Numerical solutions are calculated using FORTRAN code with $\Delta t = 10$ msec. Recall that the combined model has been simplified by assuming spherical symmetry. This idealizes the islet model, and the discretization of the diffusion term implies coupling between 'shells' of different radii.

| Symbol | Value | Symbol | Value |
|---|---|---|---|
| $g_{Ca}$ | 3.6 | $\theta_m$ | 12 mV |
| $g_K$ | 10 | $V_m$ | -20 mV |
| $g_S$ | 4 | $\theta_n$ | 5.6 mV |
| $\tau$ | 20 msec | $V_n$ | $-17$ mV |
| $\tau_S$ | 35000 msec | $\theta_S$ | 10 mV |
| $V_{Ca}$ | 25 mV | $V_S$ | $-38$ mV |
| $V_k$ | $-75$ mV | $\lambda$ | 0.9 |
| $D$ | 0 - 1500 pS $\mu$m$^2$ | $c_1$ | 2 |
| $c_2$ | 1.125 | $m$ | 3 |
| $n$ | 16 | | |
| $D_G$ | $0.673 \times 10^{-5}$ cm$^2$ | $a$ | 100 $\mu$m |
| $\rho$ | 0.02 | $R_{max}$ | 0.52 mM/s |
| $K_m$ | 17 mM | $k$ | $0.1 - 1.0$ $\mu$m$^{-1}$ |
| $p$ | $0.1 - 1.0$ | $G_{bath}$ | 0 - 30 mM |

Table 2.1: Parameter values for the combined model of islet electrical activity and glucose diffusion.

At each time step, the system is solved numerically in two parts. First, the equations representing glucose diffusion, (2.15) and (2.16), are solved, since they are independent of the remaining equations (2.12)–(2.14). Then the solution to equations (2.12)–(2.14), representing the islet model, can be calculated with the updated value of $\bar{g}_e$.

The glucose diffusion component of the combined model, (2.15) and (2.16), is solved in two parts as well. Equation (2.15), describing the extracellular glucose concentration, is of reaction-diffusion type, where the glucose transport function is the reaction. The diffusion term is discretized using the central difference

approximation and dealt with implicitly. The reaction portion of the equation is dealt with explicitly by using the values of $\bar{g}_e$ and $\bar{g}_i$ from the previous time step. Equation (2.16) is an ordinary differential equation, and is solved explicitly. For the spatial discretization of (2.15) and (2.16), we use $\Delta r = 2$ $\mu$m.

The electrical activity component of the combined model, given by (2.12)-(2.14), proved to be more difficult to approximate, due to the stiff nature of the system. During the silent phase of a burst, a relatively large time step can be used when approximating a solution, but during the active phase of the burst a smaller time step is required to accurately reflect the fast dynamics of the current balance equation. To solve (2.12)-(2.14), the method of lines is used to return the system of partial differential equations to a system of ordinary differential equations again. Then the Gear algorithm is implemented to solve the resulting system of ODEs. The benefit of the Gear method is that it uses a variable time step, which handles the stiffness of the system. We use a spatial step of $\Delta r = 10$ $\mu$m for this portion of the model, roughly reflecting a $\beta$-cell diameter. Recall that we use $\Delta r = 2$ $\mu$m for the diffusion component of the model. Therefore, the glucose value used to approximate the solution for each 10 $\mu$m 'shell' of the electrical activity component of the model is taken to be a weighted average, weighted by the volumes of each 2 $\mu$m shell, of $g_e$ values throughout the shell. This method of obtaining the glucose value could easily be replaced with $g_i$ or be modified to reflect the location of glucose receptors in the cells.

The model described is a step towards understanding the initiation of insulin secretion and obtaining a more complete understanding of islet electrical activity. In Chapter 3, we will discuss the results of various parameter studies of the combined model. The main focus is centered around testing the hypothesis of Bertram and Pernarowski in [6]: does the time required for glucose to diffuse into the islet contribute to the delay in the onset of electrical activity observed

experimentally when an islet is exposed to a stimulatory glucose bath?

# Chapter 3

# Results from the Combined Model

In this chapter, we highlight some of the interesting, physiologically relevant results obtained when numerical solutions of the combined electrical activity and diffusion model were computed. In most simulations, the islet is first exposed to a glucose-free bath for 1 minute, to ensure the solution begins at a steady state. At $t$=1 minute, the addition of glucose to the bath is simulated by a step increase in $G_{bath}$. The delay in the onset of electrical activity is recorded. We are interested in the dependence of this delay on the coupling strength, $D$, and the glucose bath concentration, $G_{bath}$. In other simulations, the islet is exposed to a uniform glucose bath, and then several step changes in $G_{bath}$ are applied, mimicking typical physiological experiments. All parameter values are as in Table 2.1 with values of permeability and porosity of $k = 0.1\ \mu\text{m}^{-1}$ and $p = 0.1$ respectively.

In most cases, we observe a delay, as predicted by Bertram and Pernarowski [6], in the onset of electrical activity after increasing the glucose bath concentration to a stimulatory level. An example of such a delay is discussed in Section 3.1. However, if the bath is at a very high concentration ($>$ 17 mM), there is no

apparent delay in the onset of electrical activity. In Section 3.2, we consider the effects of varying the coupling strength through the parameter $D$. Reducing the coupling strength between $\beta$-cells is also found to decrease the delay. Next, in Section 3.3, a similar study is conducted in which the glucose bath concentration is varied and the delay is observed. The change in delay is explained by considering the weighted-average glucose distribution throughout the islet both before bursting begins, and at the onset of bursting electrical activity. The size of the islet is increased from 100 $\mu$m to 200 $\mu$m in Section 3.4. The delay in the onset of electrical activity was longer for the larger islet. Next, in Section 3.5, we consider the average glucose level throughout the islet when bursting begins. Finally, in Section 3.6, a paradigmatic physiological experiment is simulated.

## 3.1 Delay in onset of electrical activity

In [6], Bertram and Pernarowski hypothesize that the delay between the time when an islet is first exposed to a stimulatory glucose bath concentration and the beginning of the characteristic electrical response is caused, at least in part, by the time required for glucose to diffuse into the islet. The diffusing glucose is transported into the $\beta$-cells and metabolized, producing ATP from ADP. This increase in ATP/ADP ratio reduces the conductivity of the ATP-regulated $K^+$ channel, blocking the outflow of $K^+$ ions, and depolarizing the cells. This initiates the excitability of the $\beta$-cells. Since the $\beta$-cells on the periphery are exposed to glucose first, they are the first to become active. This begins a chain reaction, as the active cells attempt to recruit their nearest neighbours via the gap junctions. However, if sufficient glucose has not yet reached the neighbouring cells, the influence of the active cells on the periphery may not be enough to excite the inner cells. For this reason, the delay in the onset of islet bursting seems to be due to the time required for glucose to diffuse into the islet.

In Figure 3.1, we illustrate an example of a delay. The figure displays the membrane potential for a cell located at 10 $\mu$m (solid line) and at 100 $\mu$m (dashed line) in an islet of radius 100 $\mu$m. First, the simulated islet is stabilized in a glucose-free bath for 1 minute, then exposed to a glucose bath of 10 mM. The plot indicates a delay of about 377 seconds between glucose application and the onset of islet electrical activity.

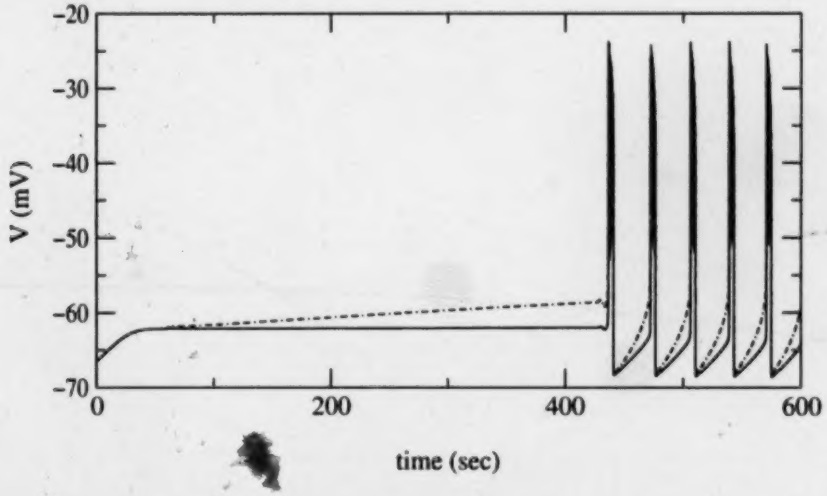


Figure 3.1: Example of the delay between introducing the glucose bath of 10 mM at 60 sec, and the onset of electrical activity in a 100 $\mu$m islet, where $D$=100 pS $\mu$m$^2$. Membrane potential is taken at a radius of 10 $\mu$m (solid line) and a radius of 100 $\mu$m (dashed line).

This delay can be explained by considering local glucose levels throughout the islet at various times, as shown in Figure 3.2. Recall that the glucose concentration used to calculate the membrane potential of each 10 $\mu$m shell is a weighted-average ($G_{avg}$) of the extracellular glucose concentration every 2 $\mu$m, weighted by the volumes of each 2 $\mu$m shell, as described in Section 2.5. The $G_{avg}$ for the 90-100 $\mu$m shell is plotted at radius of 100 $\mu$m, and so on. In Fig-

ure 3.2, $G_{avg}$ is given at 30, 90, and 377 seconds after exposure to the glucose bath.

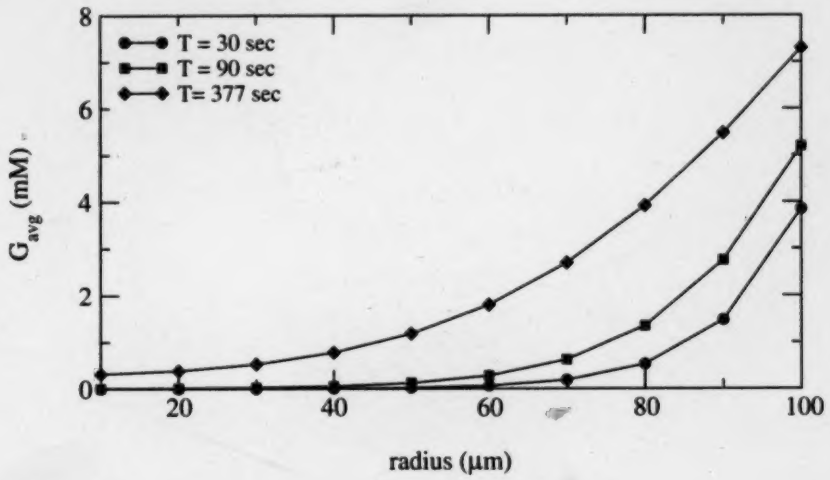


Figure 3.2: Weighted-average glucose distribution throughout the islet 30, 90 and 377 seconds after exposure to a bath glucose of 10 mM. Computations carried out for $D$=100 pS $\mu$m$^2$, with other parameters as in Table 2.1.

At $t$=30 seconds, $G_{avg} < 4$ mM in every shell. Individual cells require a local glucose concentration of at least 5.3 mM to become active. Thus, none of the shells see sufficient glucose to initiate electrical activity, and the entire islet remains silent.

After 90 seconds, the membrane potential for the cells in the outer shell (radius 90-100 $\mu$m) is computed using a $G_{avg}$ of just over 5 mM, therefore the outer shell would be active or bursting if it were not electrically connected to any other shells. This was confirmed by removing all coupling in the model. However, the adjacent shell (80-90 $\mu$m) is exposed to a $G_{avg}$ of less than 3 mM, and would not be bursting on its own. Since the outer shell is just becoming active at an average glucose of just over 5 mM, it is not enough to recruit the remainder of the islet

at intermediate coupling ($D = 100$ pS $\mu$m$^2$), and the islet remains silent.

Finally, over 6 minutes after the introduction of the stimulatory glucose bath the islet begins to burst in synchrony. The average glucose distribution is much more uniform. The outermost shell is now exposed to a $G_{avg}$ over 7 mM, with the adjacent shell exposed to about 5.5 mM. Even though the remainder of the islet is exposed to a $G_{avg}$ less than 5 mM, the large volume of the two active shells on the periphery recruit the otherwise inactive cells in the interior and initiate bursting. For the intermediate coupling strength used, there is no noticeable lag in the activation of the innermost shell relative to the outermost shell. The islet bursts are synchronized, although the outer shell does begin to depolarize gradually before bursting is initiated.

## 3.2 Effect of coupling strength on the delay

In this section, we consider the effects of changing the coupling conductance, reflected in changing the parameter $D$ (via (2.4)). As the coupling strength $D$ increases, the delay in the islet's electrical response to glucose exposure also increases. In Figure 3.3, we illustrate some examples of the temporal change in membrane potential as the parameter $D$ is varied. Simulations are computed for a glucose bath concentration of 10 mM, which is applied after $G_{bath}$ is set to 0 mM for the first 60 seconds as before.

In Figure 3.3 (a), we consider the case of very weak coupling, $D$ =1 pS $\mu$m$^2$ or $g_c$= 0.01 pS. The outermost shell, from 90-100 $\mu$m and represented by the dashed line, begins to burst alone about one minute after the glucose bath application. The coupling is not strong enough to synchronize the electrical activity, and the innermost shell, from 0-10 $\mu$m and represented by a solid line, remains silent.

In Figure 3.3 (b), the parameter $D$ is increased to 10 pS $\mu$m$^2$. Now coupling is strong enough to synchronize bursting in the islet. Both the innermost and

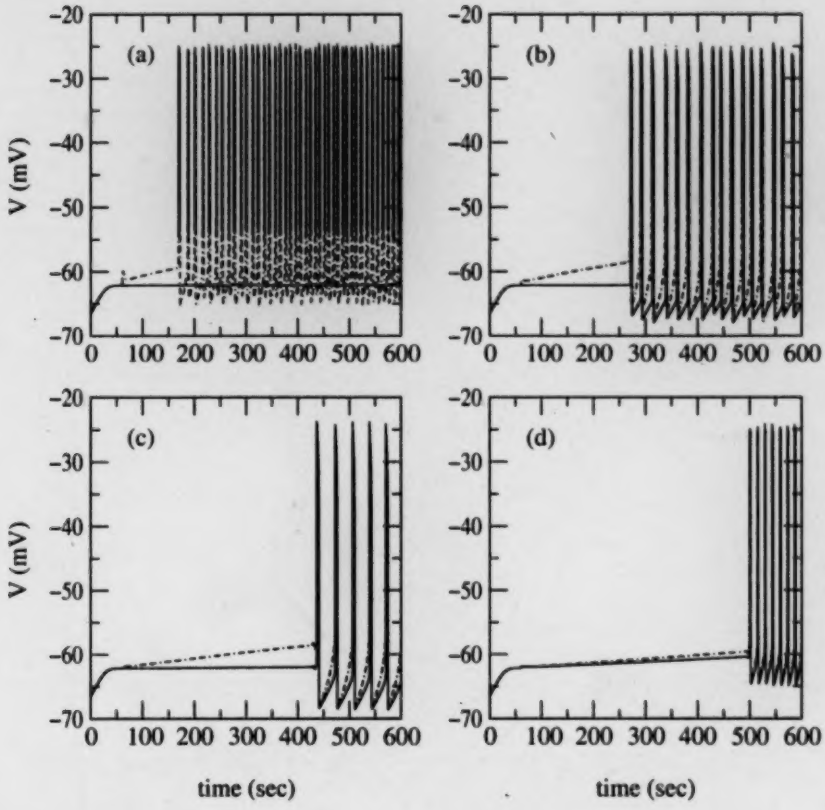


Figure 3.3: Examples of the delay in onset of islet electrical activity as the parameter $D$ is varied, when a glucose bath of 10 mM is introduced at 60 sec. Membrane potential is measured for the innermost (solid line) and outermost (dashed line) shells, for (a)$D$=1, (b) $D$=10, (c) $D$=100, (d) $D$=1500 pS $\mu$m$^2$.

outermost shells begin bursting at approximately the same time, over 4 minutes after the introduction of a 10 mM glucose bath. The delay increases to over 6 minutes when $D$ is further increased to 100 pS $\mu$m$^2$ as illustrated in Figure 3.3 (c).

With extremely strong coupling, a collection of cells responds as the average cell would. In Figure 3.3 (d), $D$=1500 pS $\mu$m$^2$, and we plot the response of the resulting 'super cell' to the glucose gradient caused by the glucose diffusion

process. The delay increases to over 7 minutes.

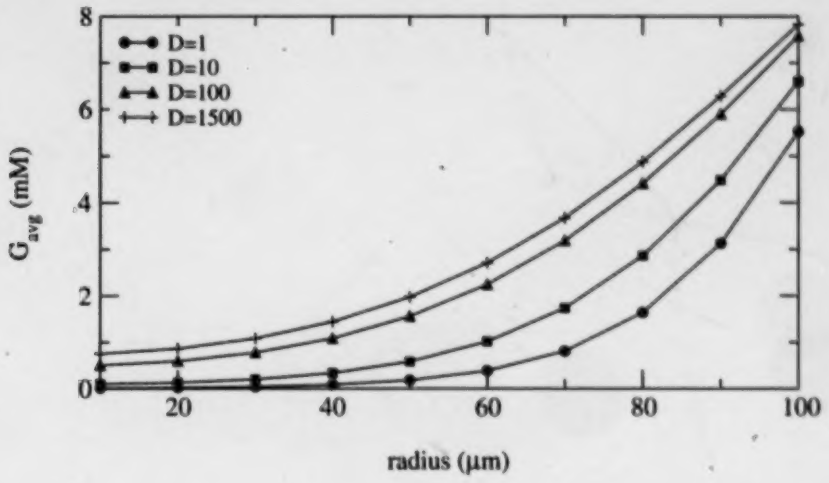


Figure 3.4: The glucose distributions at which the outermost shell in the islet begins bursting when exposed to a bath of 10 mM glucose at $t$ =60 sec as the coupling strength parameter $D$ is adjusted from 1, 10, 100 to 1500 pS $\mu m^2$, corresponding to Figure 3.3.

In order to explain the increase in delay with increased coupling strength, we consider the weighted-average glucose levels throughout the islet at the times when bursting in the outermost shell begins, corresponding to the plots in Figure 3.3. There is no significant difference in the time that bursting begins between the outer and inner shells, except for very weak coupling. Since very weak coupling is not physiologically important, we may use the time at which bursting begins in the outermost shell as a measure of the time at which bursting begins within the islet. In Figure 3.4, we record the values of $G_{avg}$ in each shell at the onset of bursting for the cases $D$=1, 10, 100, and 1500 pS $\mu m^2$.

For $D$ =1 pS $\mu m^2$, the outer shell begins bursting when $G_{avg}$=5.5 mM. As glucose begins to diffuse, the majority of cells inside the islet are exposed to $G_{avg}$

much less than 5, and would be silent if isolated. In this case, the weak coupling strength is not strong enough for the silent shells in the interior to prevent the outer shell from bursting, or for the outer shell to recruit the inner shells which remain silent. The islet is not in synchrony.

For increasing $D$, the many silent cells in the interior exert a greater influence over the neighbouring cells and prevent the islet from bursting until a higher fraction of shells are exposed to superthreshold glucose levels. This is the case for high values of $D$, as in Figure 3.3 (c) and (d). In each of these cases, the graph of the distribution of $G_{avg}$, at the time when the islet begins bursting, shows that the two outermost shells have a $G_{avg}$ greater than 5.5 mM, and therefore would be active. A domino effect occurs as the active and larger (in terms of volume) outer shells recruit the neighbouring shells until the entire islet is bursting in synchrony. The inner shells are activated so quickly that there is no noticeable delay in the bursting activity between the inner and outer shells.

The monotone increasing relationship between the parameter $D$ and the observed delay in the onset of electrical activity is illustrated in Figure 3.5. The delay is shown to vary most drastically for values of $D$ between 1 and 50 pS $\mu m^2$, then saturates at a plateau of a delay of 7 minutes for high values or $D$.

## 3.3 Effect of glucose bath concentration on the delay

In this section, we consider the effects of varying the glucose bath concentration, $G_{bath}$. As $G_{bath}$ is increased, the delay in the islet's electrical response to glucose exposure decreases. Intuitively this makes sense, since a higher glucose bath results in a higher glucose gradient across the acinar layer of the islet, and therefore diffusion across the outer layer is faster. The outer shells are more quickly

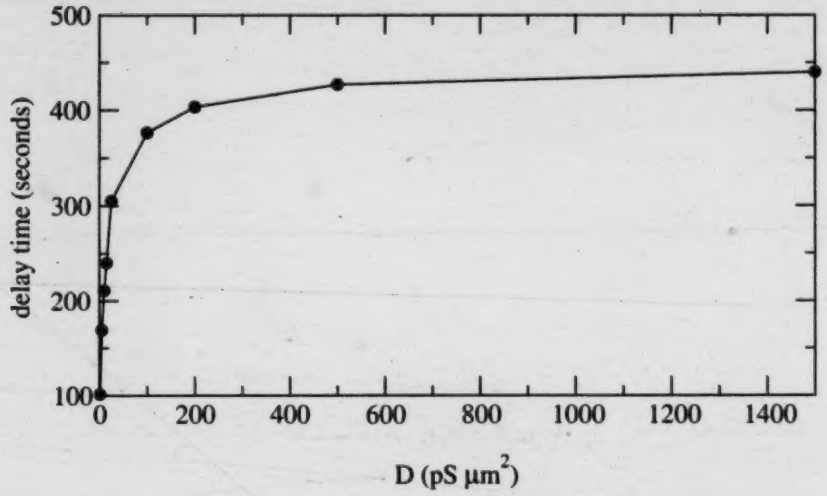


Figure 3.5: Delay in onset of electrical activity of the outermost shell after the islet is exposed to a bath of 10 mM glucose at 60 sec as the coupling strength parameter $D$ is varied from 1 to 1500 pS $\mu m^2$.

exposed to a stimulatory glucose concentration and become active. In addition, for high $G_{bath}$ concentrations, the outer shells are exposed to 'super'stimulatory glucose concentrations, i.e., the outer shell may be exposed to an average glucose level of over 7 mM within two seconds of the introduction of the glucose bath. At superthreshold average glucose concentrations, the outer shells are 'more' active than at near threshold concentration, and can more readily influence neighbouring shells to begin bursting.

In Figure 3.6, we illustrate some examples of the delay for different glucose bath concentrations. Simulations are computed for an intermediate coupling strength of $D$=100 pS $\mu m^2$, with the various $G_{bath}$ concentrations applied after the islet is stabilized in a glucose-free bath for 60 seconds. For $G_{bath}$=10 mM there is a long delay of about 7 minutes before bursting begins, as depicted in Figure 3.6 (a). The delay decreases significantly to approximately 3 minutes

and 2 minutes when $G_{bath}$ is increased to 13 mM and 15 mM in Figure 3.6 (b) and Figure 3.6 (c) respectively. In Figure 3.6 (d), it appears that there is no noticeable delay when $G_{bath}$=16.5 mM. However, we believe the initial burst may be a transient, and therefore we examine the situation more closely.

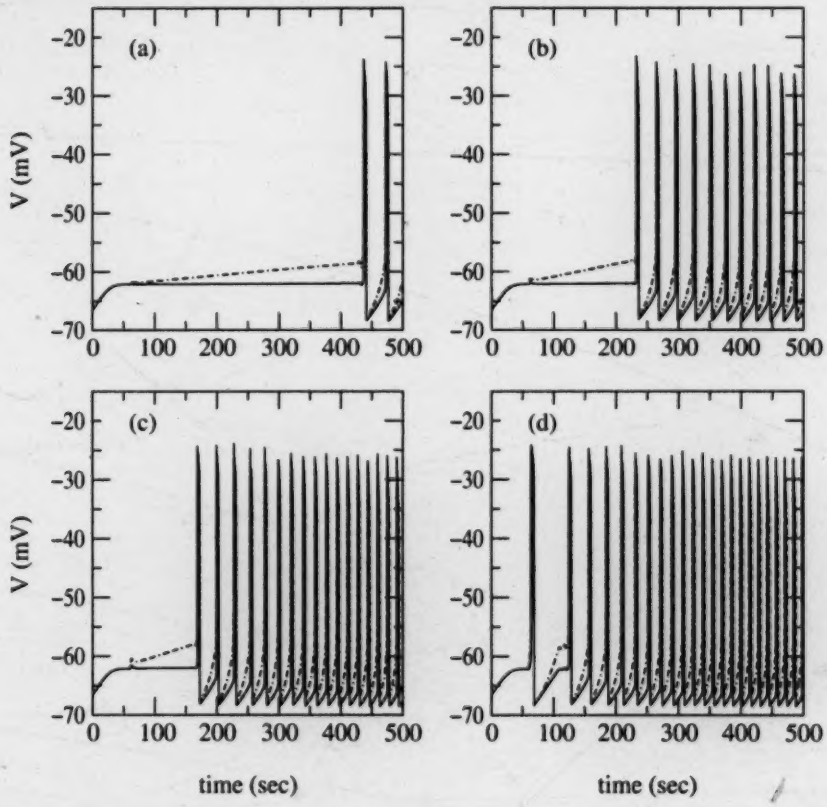


Figure 3.6: Examples of the delay in onset of islet electrical activity as the glucose bath concentration introduced at 60000 msec and varied from 10 mM to 16.5 mM and for $D$=100 pS $\mu$m$^2$. Membrane potential is measured for the innermost (solid line) and outermost (dashed line) shells, for (a) $G_{bath}$=10 mM, (b) $G_{bath}$=13 mM, (c) $G_{bath}$=15 mM, (d) $G_{bath}$=16.5 mM.

In Figure 3.7, the plot of Figure 3.6 (d) is redrawn on a shorter time scale. The

initial burst occurs only seconds after the glucose bath of 16.5 mM is introduced. Notice that the initial burst is longer than the others, and that the first silent phase is also very long compared to the bursting pattern from then on. The glucose levels at the time of the proposed 'transient' burst and at the beginning of the second burst are illustrated in Figure 3.8.

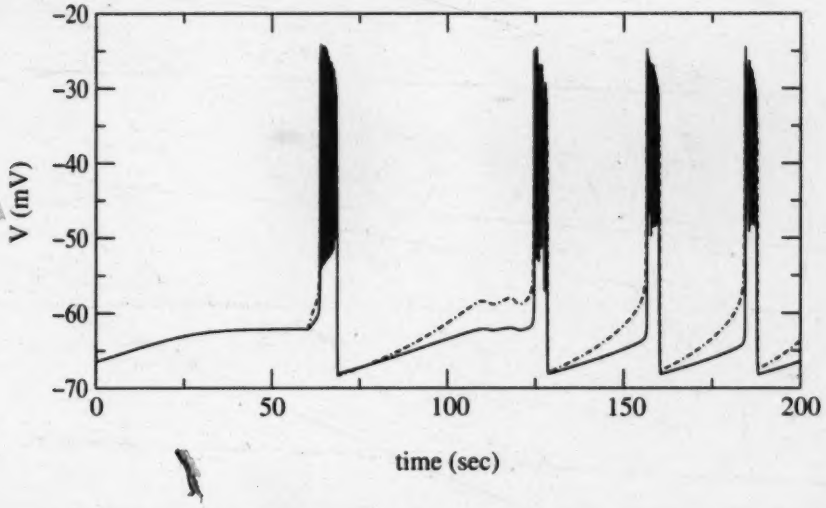


Figure 3.7: $G_{bath}$ = 16.5 mM applied at 60 seconds for $D$ = 100 pS $\mu$m$^2$.

Only 3.7 seconds after the introduction of the glucose bath of 16.5 mM, the outer shell is exposed to a $G_{avg}$ of almost 5 mM and begins to depolarize. However, the average glucose throughout the inner shells is less than 1.5 mM, which seems much too low for bursting to begin, as was the case in Figure 3.2. When the second burst begins at 124.5 seconds, approximately 1 minute later, $G_{avg}$ is about 8 mM in the outer shell, and 4 mM in the adjacent shell. It seems reasonable that, at this point, the outer shell has a strong enough influence to recruit the neighbouring shell. This initiates a chain reaction, by which the outer shells recruit the neighbouring inner shell to burst. The outer shells have an increasingly stronger influence over the adjacent inner shell due to the increasing volume ratio.

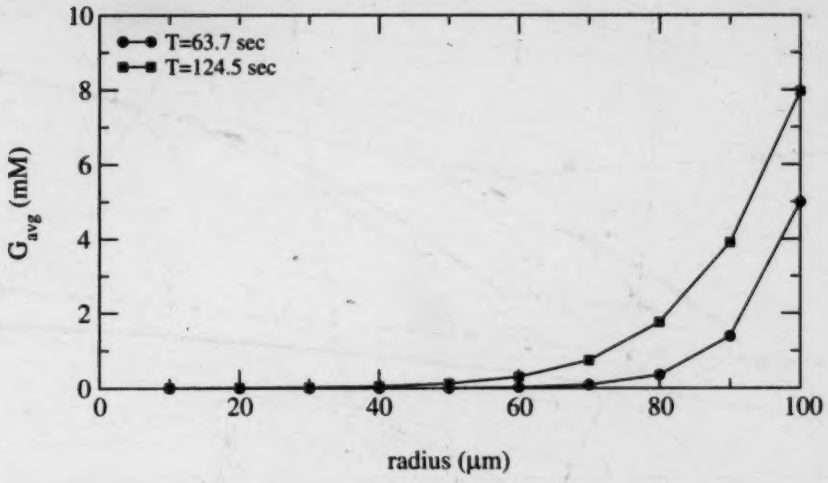


Figure 3.8: For $G_{bath}$ = 16.5 mM the weighted-average glucose concentration throughout the islet is given at 63.7 seconds and at 124.5 seconds corresponding to the onset of the first and second bursts respectively.

For example, in an islet of radius 100 $\mu$m, the innermost shell has only about 1/7 the volume of its nearest neighbour.

The relationship between the delay and the glucose bath concentration is shown in Figure 3.9. The solid line and bullets represents the delay between the glucose bath application and the beginning of regular bursting, where the initial burst is considered to be a transient if it occurs directly after the introduction of the glucose bath when glucose concentrations are substimulatory. The dashed line and stars represents the delay between the glucose bath application and the first burst. There is a drastic step change in delay between $G_{bath}$=16 mM and $G_{bath}$=16.5 mM when the proposed transient initial burst is considered. In contrast, when the transient is not included the decrease in delay with increasing $G_{bath}$ is smooth.

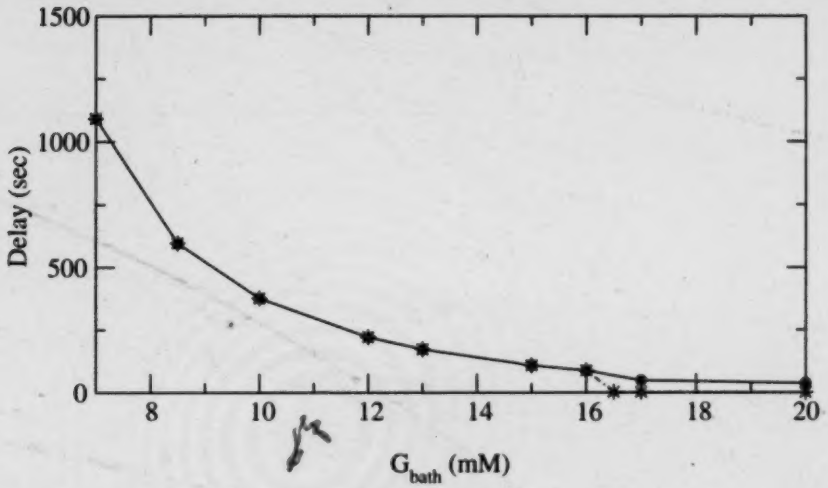


Figure 3.9: Delay in onset of electrical activity when islet is exposed to $G_{bath}$ from 7 mM to 20 mM, at 60 sec for $D = 100$ pS $\mu m^2$.

## 3.4 Effect of the islet radius on the delay

In this section, the radius of the simulated islet is doubled, from 100 $\mu$m to 200 $\mu$m. Now the outer shell is much farther away from the inner shells and gap junction connections have a reduced effect. We are interested in how the delay in the onset of bursting will change with the increased islet size, as well as possible changes in synchronization of islet electrical activity.

To reflect the larger size of the islet, the function relating the glucose sensing-parameter $R$ of the K(ATP) channel, to the weighted-average extracellular glucose concentration, in equation (2.10), had to be recalibrated. The values of $c_1 = 2.2$ and $c_2 = 1.33$ were selected for the 200 $\mu$m islet, with values of $m$ and $n$ unchanged.

In Figure 3.10 (a), we illustrate an example of the bursting behaviour exhibited by an islet of radius 200 $\mu$m (exposed to a glucose-free bath for 1 minute first), after a step increase to $G_{bath}$=13 mM for $D$ =100 pS $\mu m^2$. In Figure 3.10 (b),

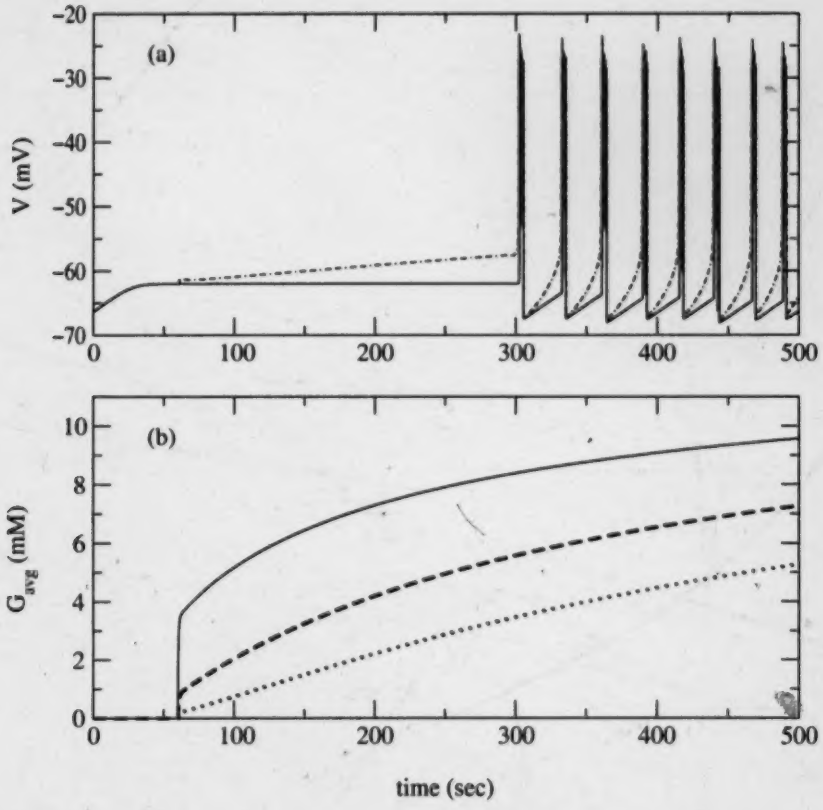


Figure 3.10: (a) Delay in the onset of bursting for $G_{bath}$=13 mM applied at 60 sec, for an islet of radius 200 $\mu$m and $D$=100 pS $\mu$m$^2$. (b) $G_{avg}$ in the three outermost shells as a function of time.

the corresponding $G_{avg}$ values are plotted for the 3 outermost shells, since the outer shells are most important in the initiation of bursting. The 190 – 200 $\mu$m shell is represented by a solid line, the 180 – 190 $\mu$m shell by a dashed line, and the 170 – 180 $\mu$m shell by a dotted line. Figure 3.10 (a) shows that the delay between the glucose bath application and the beginning of islet electrical activity is approximately 4 minutes. This is significantly longer than the less than 3-minute delay in the onset of bursting described in Section 3.3, for an islet of

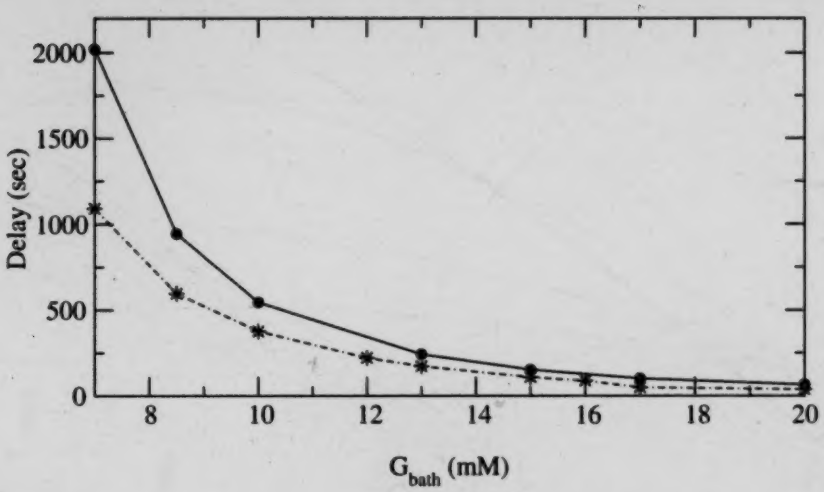


Figure 3.11: Delay in the onset of electrical activity when a 200 $\mu$m islet(solid line) is exposed to $G_{bath}$ from 7 mM to 20 mM, compared to the delay observed for a 100 $\mu$m islet (dashed line), for $D = 100$ pS $\mu$m$^2$.

100 $\mu$m in the same situation. A comparison of the delay in the onset of bursting for islets of radius 100 $\mu$m and 200 $\mu$m is illustrated in Figure 3.11. The delay is consistently higher for the larger islet, represented by the solid line and bullets, in relation to the smaller islet, represented by the dashed line and stars. In this plot, the delay is plotted for the time at which the outermost shell begins bursting, not including apparent transient bursts. For the intermediate value of coupling used to determine the delay, there was no significant difference in the onset of bursting between outer and inner shells.

In Figure 3.10 (b), $G_{avg}$ rises almost instantly in the three outer shells when the glucose bath of 13 mM is applied. When bursting begins at about $t$ =300 seconds, Figure 3.10 (b) shows that the two outermost shells would be bursting easily on their own with average glucose levels of approximately 6 mM and 8 mM. The 170-180 $\mu$m shell only has $G_{avg} \approx 3$ mM and, along with the remaining

inner shells, would be silent if isolated. Therefore, at about 6 and 8 mM the two outermost shells are sufficiently active to initiate bursting throughout the islet. This implies that approximately 1/3 of the total islet volume is active when bursting begins. However, it is worth noting that the two outer shells are not just becoming active, but are 'super'active. As seen in Figure 3.10 (b), at about $t$=250 sec, the two outer shells have $G_{avg} > 5$ mM, and would be bursting if isolated, but this is not enough to cause the entire islet to burst, especially since glucose has not yet diffused as far as the innermost shells. In Figure 3.12, the distribution of $G_{avg}$ throughout the islet is plotted at $t$=300 seconds, and it can be seen that a large part of the islet has $G_{avg} < 1$ mM. Although $G_{avg}$ is far from uniform at $t$=300 seconds, synchronized bursting begins for an intermediate coupling strength of 100 pS $\mu$m$^2$.

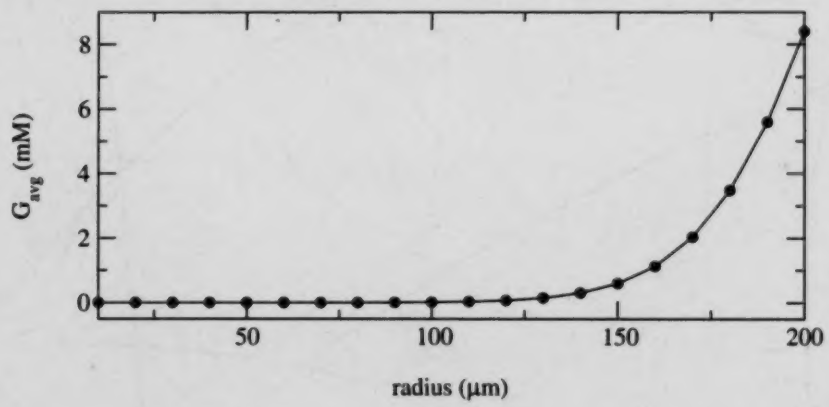


Figure 3.12: $G_{avg}$ at the onset of electrical activity ($t$=300 seconds) when an islet of radius 200 $\mu$m is exposed to $G_{bath} = 13$ mM at 60 seconds for $D = 100$ pS $\mu$m$^2$.

## 3.5 Average glucose concentration within the islet at the onset of bursting

Previously, we briefly considered the volume of 'active' shells (those with $G_{avg} > 5.3$ mM) required for bursting to occur. However, quantifying this relationship is not straightforward, as there is no single fraction of active shells that will cause bursting. In Section 3.4, it was stated that for a 200 $\mu$m islet exposed to a glucose bath of 13 mM, bursting began when the volume of active shells was approximately one third of the total islet volume. The fraction of active cells required to initiate bursting depends heavily on how 'active' the shells are. In other words, shells exposed to an average glucose significantly higher than 5.3 mM are more successful in recruiting neighbouring shells than shells just above the 5.3 mM threshold. In the first example of a delay considered in Section 3.1, a 100 $\mu$m islet was exposed to a glucose bath of 10 mM. In this case, almost one half of the volume of the islet was active before bursting began. For very high glucose bath concentrations, fractions of active shells required to initiate bursting will be less than one third.

In this section, we consider the weighted-average glucose throughout the islet at the onset of bursting. We found that as the coupling strength parameter $D$ was varied from weak to very strong coupling, the average glucose throughout the islet required to initiate bursting increased from a subthreshold level, much less than 5.3 mM, to approximately 5.3 mM, which is the glucose concentration required to initiate bursting in a single $\beta$-cell, or a 'super' cell. This relationship is illustrated in Figure 3.13, for $G_{bath}$=10 mM in an islet of radius 100 $\mu$m. The glucose concentration of 5.3 mM, corresponding to the threshold value for bursting in a single cell or 'super' cell is represented by the dashed line.

From a physiological point of view, it is interesting to note that the average

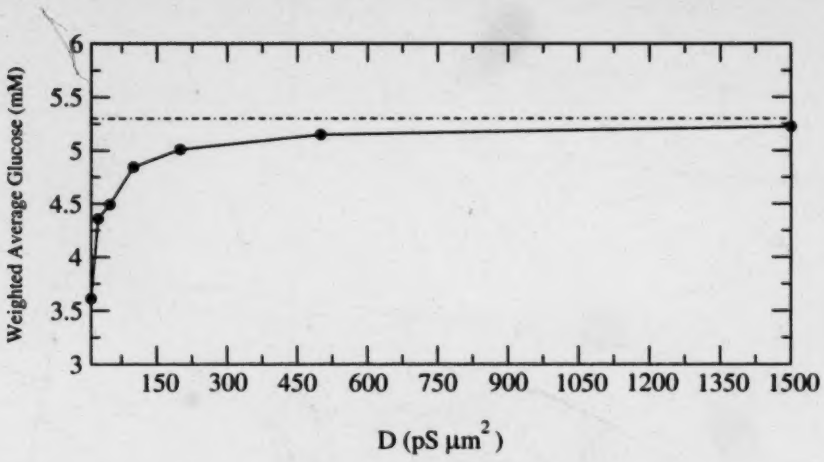


Figure 3.13: Weighted-average glucose throughout the islet at the onset of bursting as coupling strength is varied for $G_{bath}$=10 mM. As coupling strength increases, average glucose tends to the average glucose required to initiate bursting in a single cell, or a 'super' cell.

glucose concentration required to initiate bursting in an islet at an intermediate coupling strength is less than the average glucose required to initiate bursting in a islet when coupling is unusually strong. Therefore, $\beta$-cells are more efficient in responding to the glucose signal when they are coupled together with intermediate coupling conductances.

In Figure 3.14, we consider the relationship between $G_{bath}$ and the weighted-average glucose throughout the islet at the onset of bursting for an intermediate coupling strength of $D$=100 pS $\mu$m$^2$. As the glucose bath concentration changes, the weighted-average glucose throughout the islet at the onset of bursting also changes. In particular, for very high values of $G_{bath}$, the outer shells are exposed to glucose levels much greater than 5.3 mM very quickly, and have greater influence over neighbouring shells. Therefore, the weighted-average glucose at the onset of bursting is lower than for low values of $G_{bath}$, where much more glucose has

to diffuse to initiate bursting. Note that glucose baths with concentrations less than 5.3 mM are not considered, since in these cases the islet does not exhibit electrical activity.

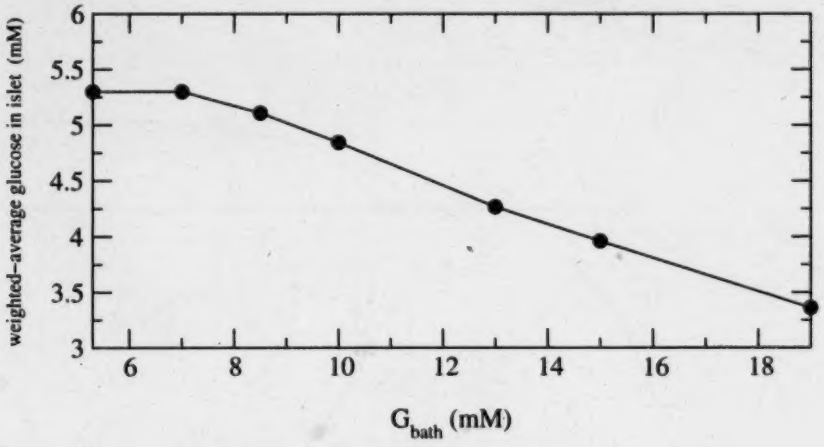


Figure 3.14: Weighted-average glucose throughout the islet at the onset of bursting as a function of the glucose bath concentration in an islet of radius 100 $\mu$m for intermediate coupling strength ($D$=100 pS $\mu$m$^2$).

The results described in this section have been obtained for an islet with a radius of 100 $\mu$m. On a final note, we mention that when the same study was carried out for an islet of radius 200 $\mu$m, we found that for high glucose bath concentrations, the weighted-average glucose throughout the islet at the onset of bursting was significantly lower than that of the smaller islet. This suggests that islet size is important, and leads us to hypothesize that for a given coupling strength, there may be an islet size that responds optimally to a glucose signal.

## 3.6 Several step changes in the glucose bath concentration

In this section, we consider a simulation using the combined model (2.12)-(2.16) based on typical physiological experiments as in [5]. The initial conditions are modified such that there is a uniform glucose bath throughout the islet initially. Several step changes in $G_{bath}$ are then applied. Numerical approximations are carried out for an islet of radius 100 $\mu$m and $D = 100$ pS $\mu$m$^2$.

Figure 3.15 (a) illustrates the scenario where a simulated islet is first stabilized at a uniform average glucose level of 5 mM, the bath and initial conditions for $g_e$ and $g_i$ are set to 5 mM. At $t$=80 seconds, $G_{bath}$ is stepped up to 7 mM and bursting begins immediately, since only a small amount of glucose is required to increase $G_{avg}$ past the threshold of about 5.3 mM. Notice that the bursts are very uniformly shaped and there is no noticeable difference between the bursting in the outermost shell (dashed line) and innermost shell (solid line). In contrast to, Figure 3.1 for example, where there is an obvious difference in the outermost and innermost shells. $G_{bath}$ remains at 7 mM from $t$=80 to 600 seconds, and $G_{bath}$ is stepped up to 11 mM at $t$=600 seconds. Figure 3.15 (b) shows this step increase. Figure 3.15 (b) is a continuation of Figure 3.15 (a) where the time from $t$=300 to $t$=500 seconds at a constant $G_{bath}$=7 mM has been omitted. Notice that when the glucose bath is increased to 11 mM at $t$=600 seconds, the plateau fraction instantly becomes larger, that is, the active phase of the burst becomes longer and the silent phase becomes shorter. In addition, a difference in the behaviour in the outer and inner shells is becoming apparent, due to the increased glucose gradient. $G_{bath}$ remains at 11 mM from t=600 to 1100 seconds, at which time $G_{bath}$ is further increased to 17 mM. Figure 3.15 (c), beginning 200 seconds after Figure 3.15 (b) ends, depicts the response to a change in $G_{bath}$ from 11 mM to 17 mM. As was

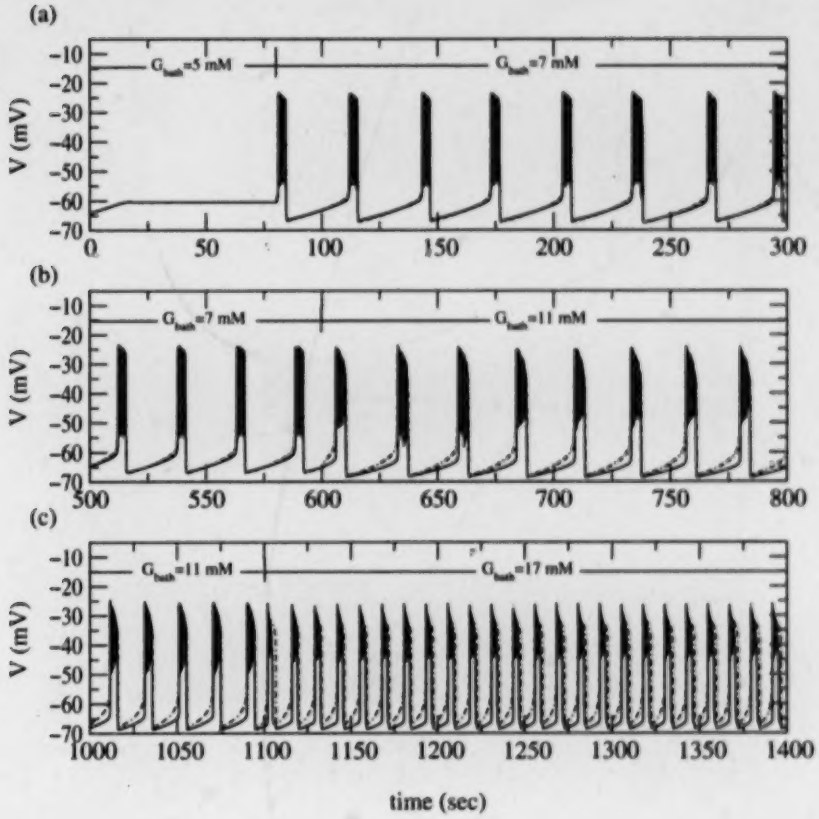


Figure 3.15: (a) Uniform $G_{avg}$ of 5 mM until $t$=80 seconds, then $G_{bath}$=7 mM applied, for an islet with radius 100 $\mu$m and D=100 pS $\mu$m$^2$. (b) $G_{bath}$ =7 mM from $t$=80 to 600 seconds, then $G_{bath}$ increased to 11 mM. (c) $G_{bath}$ =7 mM until $t$=600 to 1100 seconds, then $G_{bath}$ increased to 17 mM.

the case for the previous step increase, the plateau fraction increases immediately upon the $G_{bath}$ increase, and the bursts become less synchronized. If the $G_{bath}$ was held at a very high glucose concentration until the $G_{avg}$ was almost uniform throughout the islet, the plateau fraction would go towards 1, in other words, the islet would spike continuously. In general, Figure 3.15 illustrates the direct

response of the combined model to step changes in the glucose bath.

# Chapter 4

# Discussion and Conclusions

In this thesis, we have presented the development of a model describing the initiation of bursting electrical activity in an islet in response to diffusing glucose. In particular, we have quantified the delay in the onset of electrical activity in terms of the glucose bath concentration to which the islet is exposed, and in terms of the coupling conductance between neighbouring shells of the islet.

In Chapters 1 and 2, we presented the mathematical and physiological background required in the development of the combined model, which consists of a model of islet electrical activity connected to a model of glucose diffusion throughout the islet. Electrical activity is determined by highly nonlinear interactions of ionic currents that flow through protein channels in the $\beta$-cell membrane. Mathematical models of this phenomenon were described first for single $\beta$-cells, considered to be members of an intact islet. A model of islet electrical activity was developed by extending a general single-cell model, presented in the introductory chapter, using the techniques of Pernarowski [19]. We then considered the fact that during experiments *in vitro*, glucose enters the islets through a process of hindered diffusion. Therefore, $\beta$-cells throughout the islet are not exposed to a uniform glucose distribution. However, experiments show that $\beta$-cells within

an islet exhibit a synchronized electrical response to the introduction of glucose. Therefore, to better understand the initiation of synchronized islet electrical activity in the presence of a glucose gradient, a model of glucose diffusion, first developed by Bertram and Pernarowski [6], was incorporated into the islet model. An expression accounting for the known effects of glucose on electrical activity was introduced to connect the islet model with the model of glucose diffusion. Finally, the complete five-dimensional system of partial differential equations describing the combined model was presented, and the numerical methods used to approximate solutions to the system were described.

Simulations using the combined model were described in Chapter 3. We found that the delay in the onset of bursting after a stimulatory glucose bath is applied was a function of the glucose bath concentration, the coupling strength, and the size of the islet. It was observed that the delay increased with increases in coupling strength and islet size, and decreased with an increase in the glucose bath concentration. The predicted relationships between the delay and both islet size and glucose bath concentration are in agreement with intuition and easily could be tested experimentally. The predicted relationship between the delay and the coupling strength is an interesting, and less intuitive, result of the model. Unfortunately, it would probably be very difficult, if not impossible, to test experimentally. In addition, we considered the weighted-average glucose within the islet at the onset of bursting. We found that for an intermediate value of the coupling strength parameter $D$, the average glucose throughout the islet required for bursting was less than that required to activate a single or 'super'cell.

Admittedly, the combined model is idealistic, and although the assumption of spherical symmetry is reasonable for a first attempt, perhaps it oversimplifies the situation. Some modifications that could be made in order to model the situation more accurately include incorporating the effect of other important ion

channels found in the $\beta$-cell membrane. There are other ion channels, such as a potassium-activated calcium channel and a calcium release-activated calcium channel, that are believed to play important roles in $\beta$-cell dynamics that were neglected in this first attempt at a combined model.

In this thesis, we have focused on the role that the glucose diffusion process plays in the delay in the onset of electrical activity. Another possible contributing factor in the delay is the time required for glucose to be metabolized inside the $\beta$-cells. As previously mentioned, metabolism of glucose produces ATP, which reduces the conductance of the ATP-regulated potassium channels and eventually leads to bursting. Ultimately, the model should incorporate equations modelling the process of glucose metabolism.

We are very optimistic of possible broad-scale applications of the combined model. The model may be used in studying the effects of the diffusion of other pharmacological modulators, for which a delay in the onset of electrical activity is observed.

In conclusion, the combined model developed in this thesis provides a foundation for studying the effects of glucose diffusion on the generation of synchronized electrical activity among pancreatic $\beta$-cells within islets of Langerhans. Simulations of the combined model have yielded some interesting results on the dependence of the delay in the onset of electrical activity on pertinent model parameters. These results give insight into the relevance of electrical coupling via gap junctions and the spherical structure of the islet in being able to explain *in vitro* experimental observations. The results may have important physiological implications. We believe it would be worthwhile to test with experiments the predictions derived from our theoretical results.

# Bibliography


[1] I. ATWATER, P. CARROLL, AND M. X. LI, in Insulin Secretion, B. Draznin, S. Melmed, and D. LeRoith, eds., Alan R Liss, Inc., 1989, pp. 49–68.

[2] I. ATWATER, C. M. DAWSON, A. SCOTT, G. EDDLESTONE, AND E. ROJAS, *The nature of oscillatory behaviour in electrical activity from pancreatic β-cell*, in Hormone and Metabolic Research supplement Series No. 10, W. J. Malaisse and J. B. Täljedal, eds., Georg Thieme Verlag, Stuttgart, 1980, pp. 100–107.

[3] I. ATWATER, A. GONÇALVES, A. HERCHUELZ, P. LEBRUN, W. J. MALAISSE, E. ROJAS, AND A. SCOTT, *Cooling dissociates glucose-induced release from electrical activity and cation fluxes in rodent pancreatic islets*, J. Physiol. (London), 348 (1984), pp. 615–627.

[4] R. BAKER, A. L. HODGKIN, AND B. SHAW, *Replacement of the axoplasm of giant nerve fibers with artificial solutions*, J. Physiol., 164 (1962), pp. 330–354.

[5] P. M. BEIGELMAN, A. RIBALET, AND I. ATWATER, *Electrical activity of mouse pancreatic β-cells*, J. Physiol. (Paris), 73 (1977), pp. 201–217.

[6] R. BERTRAM AND M. PERNAROWSKI, *Glucose diffusion in pancreatic islets of Langerhans*, Biophys. J., 74 (1998), pp. 1722–1731.

[7] S. BONNER-WEIR, *Mophological evidence for pancreatic polarity of β-cells within islets of Langerhans*, Diabetes, 37 (1988), pp. 616–621.

[8] T. R. CHAY AND J. KEIZER, *Minimal model for membrane oscillations in the pancreatic beta-cell*, Biophys. J., 42 (1983), pp. 181–190.

[9] P. M. DEAN AND E. K. MATTHEWS, *Glucose induced electrical activity in pancreatic islet cells*, J. Physiol. (London), 210 (1970), pp. 255–264.

[10] B. ERMENTROUT, *XTC-a tool for modelling spatial evolution equations*, www3.pitt.edu/ phase, 1985.

[11] P. HALBAN, C. WOLLHEIM, B. BOLNDEL, P. MEDA, E. NIESOR, AND D. MINTZ, *The possible importance of contact between pancreatic islet cells for the control of insulin release*, Endocrinology, 111 (1984), pp. 86–94.

[12] A. L. HODGKIN AND A. F. HUXLEY, *A quantitative description of membrane current and its application to conduction and excitation in nerve*, J. Physiol. (London), 117 (1952), pp. 500–544.

[13] J. H. JOHNSON, C. B. NEWGARD, J. L.MILBURN, H. F. LODISH, AND B. THORENS, *The high Km transporter of islets of Langerhans is functionally similar to the low affinity transporter of liver, and has an identical primary sequence.*, J. Biol. Chem., 265 (1990), pp. 6548–6551.

[14] J. KEIZER AND G. MAGNUS, *ATP-sensitive potassium channel and bursting in the pancreatic beta cell*, Biophys. J., 56 (1989), pp. 229–241.

[15] T. A. KINARD, G. DE VRIES, A. SHERMAN, AND L. S. SATIN, *Modulation of the bursting properties of single mouse pancreatic β-cells by artificial conductances*, Biophys. J., 76 (1999), pp. 1423–1435.

[16] S. OZAWA AND O. SAND, *Electrophysiology of excitable endocrine cells*, Physiol. Rev., 66 (1986), pp. 887–952.

[17] M. PEREZ-ARMENDARIZ, D. C. SPRAY, AND M. V. L. BENNETT, *Biophysical properties of gap junctions between freshly dispersed pairs of mouse pancreatic beta cells*, Biophys. J., 59 (1985), pp. 76–92.

[18] M. PERNAROWSKI, *Fast subsystems bifurcations in a slowly varying Liénard system exhibiting bursting*, SIAM J. Appl. Math., 54 (1984), pp. 814–832.

[19] ——, *Fast and slow subsystems for a continuum model of bursting activity in the pancreatic islet*, SIAM J. Appl. Math., 58 (1998), pp. 1667–1687.

[20] E. RIESKE, P. SCHUBERT, AND G. M. KREUTZBERG, *Transfer of radioactive material between electrically coupled neurons of the leech central nervous system*, Brain Res., 84 (1975), pp. 365–382.

[21] J. RINZEL, *Bursting oscillations in an excitable membrane model*, in Ordinary and Partial Differential Equations, Lecture Notes in Mathematics 1151, B. D. Sleeman and R. J. Jarvis, eds., Springer, New York, 1985, pp. 304–316.

[22] P. RORSMAN AND G. TRUBE, *Calcium and delayed potassium currents in mouse pancreatic β-cells under voltage clamp conditions*, J. Physiol. (London), 374 (1986), pp. 531–550.

[23] A. SHERMAN, *Theoretical aspects of synchronized bursting in β-cells*, in Pacemaker Activity and intercellular communication, J. D. Huizinga, ed., 1995, pp. 323–337.

[24] ——, *Contributions of modeling to understanding stimulus secretion coupling in pancreatic β-cells*, Am. J. Physiol., 271 (1996), pp. E362–E372.

[25] A. SHERMAN AND J. RINZEL, *Model for synchronization of pancreatic β-cells by gap junctions*, Biophys. J., 59 (1991), pp. 547–559.

[26] A. SHERMAN AND J. RINZEL, *Rhythmogenic effects of weak electronic coupling in neuronal models*, Proc. Natl. Acad. Sci. USA, 89 (1992), pp. 2471–2474.

[27] P. A. SMITH, F. M. ASHCROFT, AND P. RORSMAN, *Simultaneous recordings of glucose dependent electrical activity and ATP-regulated $K^+$-currents in isolated mouse pancreatic β-cells*, FEBS Lett., 261 (1990), pp. 187–190.

[28] P. SMOLEN AND J. KEIZER, *Slow voltage inactivation of $Ca^{2+}$ currents and bursting mechanisms for mouse pancreatic β-cells*, J. Math. Biol., 127 (1992), pp. 9–17.

[29] P. SMOLEN, J. RINZEL, AND A. SHERMAN, *Why pancreatic islets burst but single β-cells do not*, Biophys. J., 64 (1993), pp. 1668–1680.

[30] R. R. WHITESELL, A. C. POWERS, D. M. REGEN, AND N. A. ABUMRAD, *Transport and metabolism of glucose in an insulin secreting cell line*, Biochemistry, 30 (1991), pp. 11560–11566.